J. Fluid Mech. (1989), *vol.* 203, 215–249
Printed in Great Britain

The propagation of two-dimensional and axisymmetric viscous gravity currents at a fluid interface

By JOHN R. LISTER† AND ROSS C. KERR†

Department of Applied Mathematics and Theoretical Physics, University of Cambridge, Silver Street, Cambridge CB3 9EW, UK

(Received 16 December 1987 and in revised form 22 August 1988)

Viscous gravity currents resulting from the introduction of fluid between an upper layer of fluid of lesser density and a lower layer of greater density are analysed. The nonlinear equations governing the spread and shape of the intrusion are formulated for the cases of intrusion at low Reynolds number between deep ambient layers and of flow over a shallow layer of viscous fluid with a rigid lower boundary. Similarity solutions of these equations are obtained in both two-dimensional and axisymmetric geometries, under the assumption that the volume of intruding fluid increases with time like t^{α}. The theoretical predictions are shown to be in reasonable agreement with experimental observations of the spreading of glucose syrups and of viscous hydrocarbons between fluid layers of differing densities. Scaling arguments are used to derive many new results for the rates of spread of intrusions in a wide variety of further situations. A compendium of spreading relations, including some previously isolated results, is derived within a coherent framework and tabulated.

1. Introduction

When fluid is introduced at the interface between two fluids, one of greater and one of lesser density, then a gravity current results: the injected fluid intrudes along the interface, driven by buoyancy forces. A gravity current will also result from the introduction of fluid at the lower boundary of a less dense fluid or at the upper boundary of a more dense fluid; here the intrusion occurs between the boundary and the ambient fluid. Such flows are ubiquitous both in nature and in industry. Most researchers have concentrated on large-Reynolds-number gravity currents such as those occurring in the atmosphere, oceans and lakes. Examples of such flows, in which there is a balance between inertial and buoyancy forces, may be found in a review by Simpson (1982). In this paper we consider low-Reynolds-number gravity currents, in which the flow is retarded by viscous rather than inertial forces. This regime has received much less attention, despite its relevance to geological applications (Kerr & Lister 1987; Huppert *et al.* 1982) and elsewhere.

In this paper we derive, in both axisymmetric and two-dimensional geometries, new solutions for the shape and rate of spread of viscous gravity currents in two situations. In §2 we first present equations for intrusion at the interface between two deep layers of viscous fluid, and for spread over a shallow layer of viscous fluid lying above a rigid boundary.

† Present address: Research School of Earth Sciences, The Australian National University, GPO Box 4, Canberra, ACT 2601, Australia.

In each case, inertial and surface-tension forces are assumed to be negligible everywhere, as are the effects of diffusion and mixing at the fluid interfaces. Similarity forms of solution are given for conditions in which the total volume of intruding fluid is proportional to t^α, where α is a non-negative constant. Thus, we include the important and interesting cases of constant volume release ($\alpha = 0$) and constant flux input ($\alpha = 1$).

The flow in the intruding fluid is analysed using the approximations of lubrication theory. In the deep-layer problem, the flow in the ambient fluid is given in terms of the boundary-integral representation of Stokes flow; the derivation of an appropriate numerical method of solution is given in Appendix C. In Appendix A §A.1 the neglect of the inertial forces is shown to be valid if $\alpha < \frac{1}{4}$ (two-dimensional) or $\alpha < \frac{3}{4}$ (axisymmetric), and $t \gg t_1$, where t_1 is the transition time at which inertial and viscous forces balance. The analysis of the shallow-layer flow is made under the assumption that the surface gravity current occupies a negligible fraction of the layer depth. The assumption is justified at large times if $\alpha < \frac{1}{2}$ (two-dimensional) or $\alpha < 1$ (axisymmetric); if α exceeds these values then the depth of the current increases until it touches the rigid bottom and the analysis of Huppert (1982) becomes applicable; the solution when α equals these values is derived in Appendix B.

In §3 we describe a series of measurements of the spread of high-viscosity glucose syrups. The experimental configurations include two-dimensional and axisymmetric geometries, fixed flux and fixed volume releases, and shallow and deep ambient fluids. The measurements are shown to be in reasonable agreement with the appropriate analytic solution. A discussion of the results is given in §4.

In Appendix A we use scaling arguments to highlight the important physical balances underlying the detailed analysis and to rederive the spreading laws of §2 to within a multiplicative constant. As we have mentioned, the scaling arguments are then used to determine the values of α and t for which the analytic theory is valid. Though the scaling arguments do not provide as much detailed information as the analytic solutions to the equations of motion, they may be used to indicate when effects other than buoyancy and viscosity may be neglected, and also to determine the rate of spread when such effects are important. We discuss the cases of surface tension and of diffusion. The flexibility of the approach allows us to cover previous studies of flow over a rigid surface (Huppert 1982; Didden & Maxworthy 1982; Maxworthy 1983), viscous flow along the free surface of a relatively inviscid fluid (Fay 1969; Hoult 1972) and intrusion into stongly stratified environments (Maxworthy 1972; Chen 1980), as well as to derive many fresh results. These results are tabulated for reference.

2. Analytic solutions

In this section we derive analytic solutions for the spread of a viscous gravity current in two particular geometries. First, we consider the intrusion of fluid with an intermediate density along the interface between two deep fluid layers in Stokes flow, far from rigid boundaries. Secondly, we discuss the spread of light fluid over a shallow fluid layer with a rigid horizontal bottom. In the following paragraphs we present the analysis that is common to these situations, before deriving the solutions in turn.

Consider a current of density ρ_0 intruding between a fluid layer of lesser density ρ_+, initially occupying the region $z > 0$, and another layer of greater density ρ_-, initially occupying the region $z < 0$ (see figure 1*a*, *b*). For the moment, we shall confine

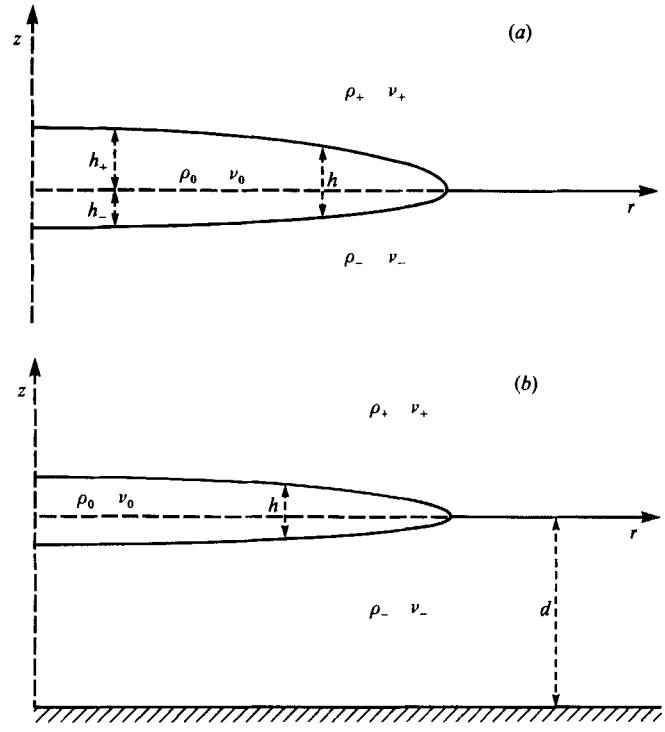

FIGURE 1. Definition sketches for the spread of an intrusion: (*a*) between two deep layers of viscous fluid; (*b*) over a shallow layer of depth d.

attention to intrusion in an axisymmetric geometry. Let the viscosities of the fluids be ν_0, ν_+ and ν_- respectively, and let the intrusion occupy $h_-(r,t) < z < h_+(r,t)$ for $0 \leqslant r \leqslant r_N(t)$. The intrusion is assumed to be of a much greater horizontal extent than vertical depth (i.e. $r_N \gg h_\pm$); this will be the case at sufficiently large times (see (A 10) in Appendix A). It is also assumed that the depth of the ambient fluid is much greater than the depth of the intrusion (see (A 11)).

The density differences between the fluids may be represented by a hydrostatic pressure

$$p_H = p_0 - \rho_+ gz - (\rho_0 - \rho_+) g\left(h_+ - \frac{\rho_- - \rho_0}{\rho_- - \rho_+} h\right) \quad (h_+ < z), \tag{2.1a}$$

$$p_H = p_0 - \rho_0 gz + \rho_0 g' h \quad (h_- < z < h_+), \tag{2.1b}$$

$$p_H = p_0 - \rho_- gz - (\rho_0 - \rho_-) g\left(h_- - \frac{\rho_+ - \rho_0}{\rho_- - \rho_+} h\right) \quad (z < h_-), \tag{2.1c}$$

where

$$g' = \frac{(\rho_0 - \rho_+)(\rho_- - \rho_0)}{(\rho_- - \rho_+)\rho_0} g, \quad h = h_+ - h_-.$$

The flow driven by the gradients of this hydrostatic pressure may be considered in two parts. Any horizontal gradients of p_H in the ambient fluid act to establish a local hydrostatic equilibrium in which the intrusion 'floats' between the two ambient fluids and h_+ and h_- are in the ratio $\rho_- - \rho_0 : \rho_0 - \rho_+$; the horizontal gradients of p_H within the intrusion cause it to spread. Since the depth of the ambient fluid is much greater than h, the local hydrostatic equilibrium is achieved on a much shorter

timescale than the subsequent lateral spread of the intrusion. This equilibrium is not disturbed by the viscous stresses caused by the spread.

Since $h \ll r_N$, the velocity in the intrusion is nearly horizontal and we may use the approximations of lubrication theory. (The breakdown of these approximations in the immediate neighbourhood of the nose of the current only affects the flow within an $O(h)$ distance of the nose. It does not, therefore, influence the global dynamics of the current, which determine the spreading rate, cf. discussion in Huppert 1982). Therefore, if surface tension and inertial forces within the intruding fluid are negligible, the velocity in the current u_0 is given by

$$\nu_0 \frac{\partial^2 u_0}{\partial z^2} = \frac{1}{\rho_0}\frac{\partial p_H}{\partial r} = g'\frac{\partial h}{\partial r}, \tag{2.2}$$

with solution

$$u_0 = U + Az + \frac{g'}{2\nu_0}\frac{\partial h}{\partial r} z^2. \tag{2.3}$$

The vertical extent of the flow in the ambient fluid will be $O(r_N)$ for the unbounded Stokes flow and d for flow over a shallow layer. Hence, the vertical scale of velocity variations will be much greater than the depth of the intrusion. Therefore, when solving for the velocities in the ambient fluid, we may replace the boundary conditions at $z = h_\pm$ by conditions at $z = 0$. Provided that ν_0 is not much less than ν_+ or ν_-, we may also neglect the variation in velocity across the intrusion in the equation of mass continuity for the intruding fluid and in the equation of continuity of velocity at $z = h_\pm$. Thus, in the region $0 \leqslant r \leqslant r_N$

$$\frac{\partial h}{\partial t} + \frac{1}{r}\frac{\partial}{\partial r}(rhU) = 0 \tag{2.4}$$

and

$$U = u_-|_{z=0} = u_+|_{z=0}. \tag{2.5}$$

The velocity of the intrusion causes bulk motion of the ambient layers. It is the solution for the motion in the ambient fluid that the analyses of the Stokes flow and shallow-layer intrusions diverge.

2.1. *Stokes flow in a deep layer*

Consider intrusion into a large volume of viscous fluid whose boundaries are at a much greater distance than the extent of the intrusion. The flow in the ambient fluid may then be treated as being unbounded.

We assume that the Reynolds number of this motion is sufficiently small that at any instant the ambient fluid is in Stokes flow given by the viscous stresses exerted at the interfaces between the intruding and ambient fluids. We use the general identity for Stokes flow (Ladyzhenskaya 1963):

$$\tfrac{1}{2}\boldsymbol{u}(\boldsymbol{x}) = -\frac{3}{4\pi}\int_{\partial V} \frac{\boldsymbol{rrr}}{|\boldsymbol{r}|^5} : \boldsymbol{un}\,\mathrm{d}A(\boldsymbol{y}) + \frac{1}{8\pi\mu}\int_{\partial V}\left(\frac{\mathbf{1}}{|\boldsymbol{r}|} + \frac{\boldsymbol{rr}}{|\boldsymbol{r}|^3}\right)\cdot\boldsymbol{\sigma}\cdot\boldsymbol{n}\,\mathrm{d}A(\boldsymbol{y}) \quad (\boldsymbol{x}\in\partial V), \tag{2.6}$$

where $\boldsymbol{r} = \boldsymbol{x} - \boldsymbol{y}$, $\mathbf{1}$ denotes the unit tensor and $\boldsymbol{u}$ is a Stokes flow with stress tensor $\boldsymbol{\sigma}$ in domain V with boundary ∂V and outward normal $\boldsymbol{n}$. When this is applied to each of the flows $\boldsymbol{u}_+$ and $\boldsymbol{u}_-$ at a point $\boldsymbol{x}$ on $z = 0$ the first integral vanishes because

$\boldsymbol{r}\cdot\boldsymbol{n} = 0$ and the left-hand sides are equal to $\frac{1}{2}U(\boldsymbol{x})$ by (2.5). We substitute for $\boldsymbol{\sigma}$ from (2.3), multiply by the viscosity and add the results to deduce that

$$U = -\frac{\rho_0 g'}{4\pi(\mu_+ + \mu_-)} \int_0^{r_N} \int_0^{2\pi} h \frac{\partial h}{\partial r'} \left(\frac{1}{|\boldsymbol{r}|} + \frac{(\boldsymbol{r}\cdot\boldsymbol{e}_r)^2}{|\boldsymbol{r}|^3} \right) \mathrm{d}\theta\, r'\, \mathrm{d}r', \tag{2.7}$$

where $\boldsymbol{y} = (r'\cos\theta, r'\sin\theta, 0)$ and $\boldsymbol{e}_r$ is a unit vector in the radial direction. Substitution of (2.7) into (2.4) yields the following nonlinear partial differential equation for h:

$$\frac{\partial h}{\partial t} = \frac{2g'\rho_0}{\mu_+ + \mu_-} \frac{1}{r} \frac{\partial}{\partial r} \left(rh \int_0^{r_N} h(r') \frac{\partial h(r')}{\partial r'} \mathscr{K}(r'; r)\, \mathrm{d}r' \right), \tag{2.8}$$

where the dimensionless kernel $\mathscr{K}$ is defined by

$$\mathscr{K}(r'; r) = \frac{r'}{8\pi} \int_0^{2\pi} \frac{1}{|\boldsymbol{r}|} + \frac{(\boldsymbol{r}\cdot\boldsymbol{e}_r)^2}{|\boldsymbol{r}|^3} \mathrm{d}\theta. \tag{2.9}$$

We solve (2.8) subject to the global continuity condition

$$2\pi \int_0^{r_N} hr\, \mathrm{d}r = Qt^\alpha. \tag{2.10}$$

While solutions to (2.8) and (2.10) may be obtained numerically from given initial conditions, it is better to observe that the problem has a similarity solution and that any solution with sufficiently smooth initial conditions will tend to this similarity form. We define

$$\eta = \eta_N^{-1} \left(\frac{2g'\rho_0}{\mu_+ + \mu_-} \right)^{-\frac{1}{5}} \left(\frac{Q}{2\pi} \right)^{-\frac{2}{5}} r t^{-(2\alpha+1)/5}, \tag{2.11a}$$

$$h(r, t) = \eta_N^{\frac{1}{2}} \left(\frac{2g'\rho_0}{\mu_+ + \mu_-} \right)^{-\frac{2}{5}} \left(\frac{Q}{2\pi} \right)^{\frac{1}{5}} t^{(\alpha-2)/5} H(\eta), \tag{2.11b}$$

where

$$\eta_N = \left(\int_0^1 H\eta\, \mathrm{d}\eta \right)^{-\frac{2}{5}}, \quad H(1) = 0.$$

Substitution into (2.8) yields the following equation for H:

$$\frac{\alpha-2}{5} H - \frac{2\alpha+1}{5} H'\eta = \frac{1}{\eta} \frac{\mathrm{d}}{\mathrm{d}\eta} \left(\eta H \int_0^1 HH' \mathscr{K}(\eta'; \eta)\, \mathrm{d}\eta' \right), \tag{2.12}$$

which in general can only be solved numerically. A numerical scheme for the solution of (2.12) is described in Appendix C. Solutions for H at various values of α and the dependence of the constant η_N on α are shown in figure 2.

In the important special case of a fixed volume release ($\alpha = 0$) we can integrate (2.12) and apply the boundary condition at $\eta = 1$ to deduce that

$$-\tfrac{1}{5}\eta = \int_0^1 HH' \mathscr{K}\, \mathrm{d}\eta' \quad (\alpha = 0). \tag{2.13}$$

Equation (2.13) shows that HH' is the stress distribution induced on a rigid disk by an axisymmetric straining motion with radial rate of strain $\frac{1}{5}$. This is a degenerate case of general linear motion past an ellipsoid given by Jeffery (1922) and Hinch (1972). Their analyses show that

$$HH' = -\frac{16\eta}{5\pi(1-\eta^2)^{\frac{1}{2}}}. \tag{2.14}$$

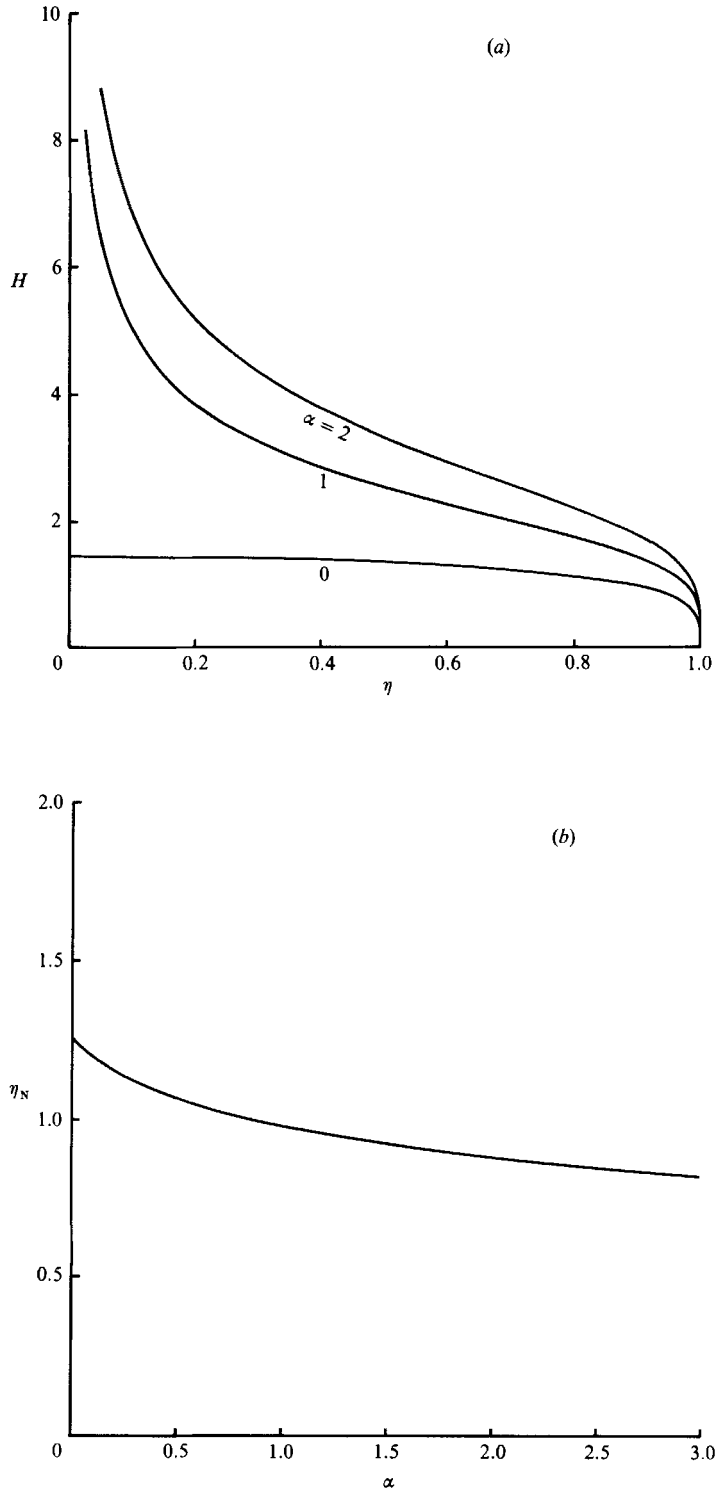

FIGURE 2. An axisymmetric gravity current, of volume Qt^{α}, spreading between two deep layers of viscous fluid. (*a*) The shape of the current; (*b*) the dimensionless length η_N of the current as a function of α.

Hence
$$H = \left(\frac{32}{5\pi}\right)^{\frac{1}{2}}(1-\eta^2)^{\frac{1}{4}}, \quad \eta_N = \left(\frac{125\pi}{128}\right)^{\frac{1}{5}}. \tag{2.15}$$

The predicted spreading law for an axisymmetric drop of constant volume is thus given by
$$r_N = \left(\frac{125}{256\pi}\frac{\rho_0 Q^2 g'}{\mu_+ + \mu_-}\right)^{\frac{1}{5}} t^{\frac{1}{5}}. \tag{2.16}$$

Note that the scaling arguments given in Appendix A can predict this answer to within the numerical constant and the dependence on the viscosity ratio μ_+/μ_-.

The analysis of a two-dimensional current, spreading symmetrically in $-x_N \leqslant x \leqslant x_N$ follows a similar line of reasoning to the above. Therefore, we only sketch below the derivation of the two-dimensional result analogous to (2.16). The equation of mass continuity of intruding fluid is
$$\frac{\partial h}{\partial t} + \frac{\partial}{\partial x}(hU) = 0, \tag{2.17}$$
with a global volume constraint
$$\int_0^{x_N} h\,\mathrm{d}x = Qt^\alpha. \tag{2.18}$$

Though the Green function for two-dimensional Stokes flow is logarithmically unbounded at infinity, the equivalent identity to (2.6) is nevertheless well-defined for the flow under consideration here, owing to the symmetry $\sigma(x) = -\sigma(-x)$ of the stress generating it. We find that
$$U = -\frac{2\rho_0 g'}{\mu_+ + \mu_-}\int_{-x_N}^{x_N} h\frac{\partial h}{\partial x'}\mathscr{K}(x';x)\,\mathrm{d}x', \tag{2.19}$$
where
$$\mathscr{K}(x';x) = -\frac{1}{4\pi}\ln|x-x'|. \tag{2.20}$$

The appropriate similarity variables are
$$\xi = \xi_N^{-1}\left(\frac{2g'\rho_0}{\mu_+ + \mu_-}\right)^{-\frac{1}{3}} Q^{-\frac{2}{3}} x t^{-(2\alpha+1)/3}, \tag{2.21a}$$
$$h(x,t) = \xi_N^{\frac{1}{2}}\left(\frac{2g'\rho_0}{\mu_+ + \mu_-}\right)^{-\frac{1}{3}} Q^{\frac{1}{3}} t^{(\alpha-1)/3} H(\xi), \tag{2.21b}$$
where
$$\xi_N = \left(\int_0^1 H(\xi)\,\mathrm{d}\xi\right)^{-\frac{2}{3}}, \quad H(1) = 0.$$

Then
$$\frac{\alpha-1}{3}H - \frac{2\alpha+1}{3}H'\xi = \frac{\mathrm{d}}{\mathrm{d}\xi}\left(H\int_{-1}^{1} HH'\mathscr{K}(\xi';\xi)\,\mathrm{d}\xi'\right). \tag{2.22}$$

Numerical solutions of this equation are shown in figure 3.

Again, in the important case of fixed volume release ($\alpha = 0$) we can integrate once and use an analogy with straining motion past a degenerate ellipsoid to solve for H. This time we find that
$$H = \left(\frac{8}{3}\right)^{\frac{1}{2}}(1-\xi^2)^{\frac{1}{4}}, \quad \xi_N = \left(\frac{[\Gamma(\frac{1}{4})]^4}{27\pi}\right)^{-\frac{1}{2}} = 0.789\ldots. \tag{2.23}$$

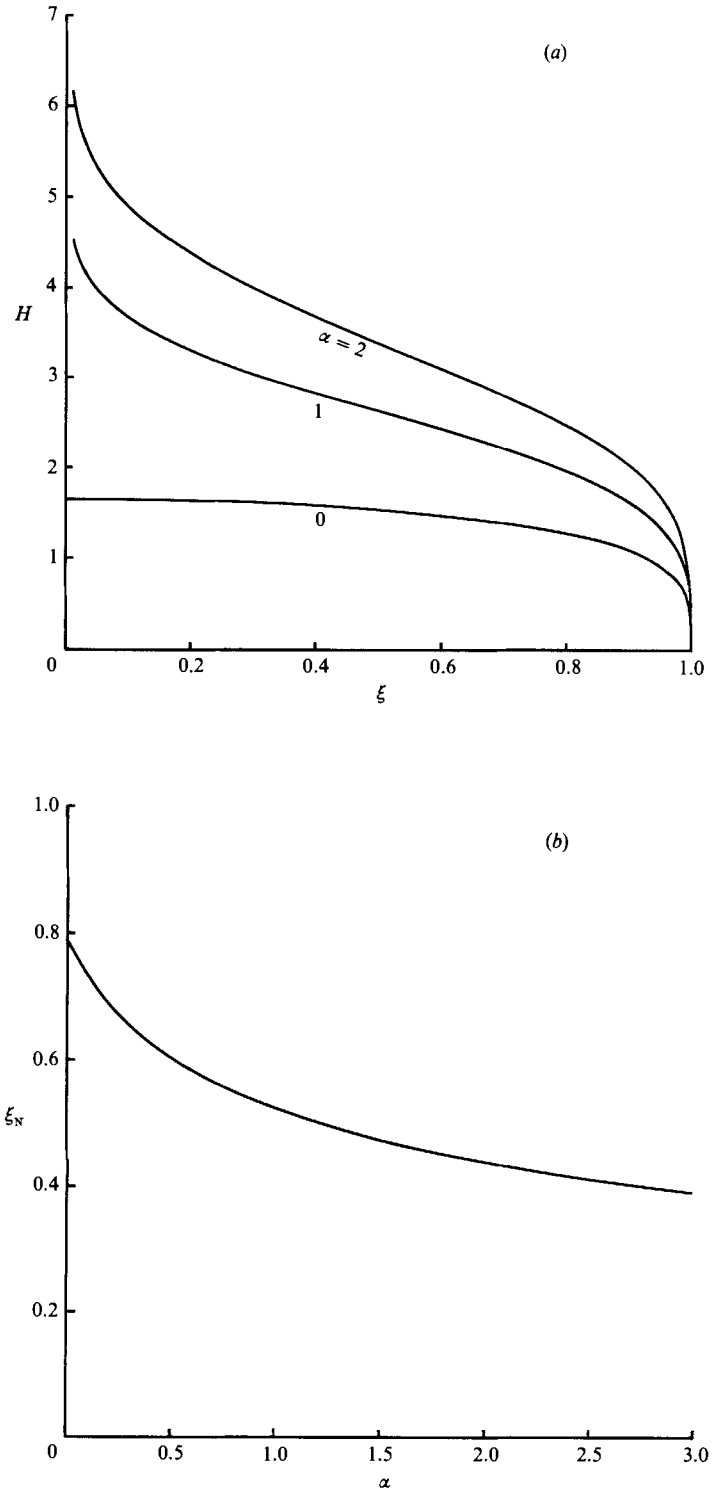

FIGURE 3. A two-dimensional gravity current, of volume Qt^{α}, spreading between two deep layers of viscous fluid. (*a*) The shape of the current; (*b*) the dimensionless length ξ_N of the current as a function of α.

The spreading law for a two-dimensional drop of constant volume is therefore given by

$$x_N = \left(\frac{2[\Gamma(\frac{1}{4})]^4}{27\pi}\frac{\rho_0 Q^2 g'}{\mu_+ + \mu_-}\right)^{\frac{1}{3}} t^{\frac{1}{3}}. \tag{2.24}$$

2.2 *Flow over a shallow layer*

Suppose now that the layer of ambient fluid in $z < 0$ is supported by a rigid horizontal boundary at $z = -d$ (figure 1*b*). We assume that $h \ll d \ll r_N$, as will be the case at sufficiently large times if $\alpha < 1$ (see Appendix A §A.1). The velocity profile within the intrusion is given by (2.3). The vertical scale of motion in the upper fluid will be much greater than d provided that $t \gg d^2/\nu_+$. We may thus neglect the stress exerted by the intrusion on the upper fluid in comparison with the stress,

$$\sigma = -\rho_0 g' h \frac{\partial h}{\partial r}, \tag{2.25}$$

exerted on the lower, shallow layer. Since $d \ll r$, the motion in the lower layer caused by this stress will be horizontal except in small regions of size $O(d)$ near $r = 0$ and $r = r_N$.

Initially, the outward motion of the intrusion causes an outward motion of the lower layer of fluid and a slight decrease in the thickness of the layer. However, the fall in the level of lower fluid soon causes a reverse pressure gradient within that layer due to the density difference $\rho_- - \rho_+$. A quasi-steady equilibrium is set up in which the reverse pressure gradient is precisely that required to ensure that there is no net flux of lower fluid through any radial cross-section. This argument is equivalent to the requirement of local hydrostatic equilibrium was discussed earlier. Therefore, the timescale for the establishment of this equilibrium which is much less than that for spread of the intrusion since $h \ll d$ and $g' < g(\rho_+ - \rho_-)/\rho_0$. The velocity profile u_- in the lower layer is driven by the surface stress σ and the reverse pressure gradient. Hence it satisfies

$$\frac{\partial^2 u_-}{\partial z^2} = \text{constant}, \quad \mu_- \frac{\partial u_-}{\partial z} = \sigma \quad (z = 0), \tag{2.26a, b}$$

$$\int_{-d}^{0} u_- \, dz = 0, \quad u_-(-d) = 0. \tag{2.26c, d}$$

The solution to (2.26) is

$$u_- = \frac{\sigma d}{4\mu_-}\left(1 + 4\frac{z}{d} + 3\frac{z^2}{d^2}\right). \tag{2.27}$$

Substituting from (2.27) and (2.25) into the continuity conditions (2.4) and (2.25) we obtain the following differential equation for $h(r, t)$:

$$\frac{\partial h}{\partial t} = \frac{g' \rho_0 d}{4\mu_-}\frac{1}{r}\frac{\partial}{\partial r}\left(r h^2 \frac{\partial h}{\partial r}\right). \tag{2.28}$$

(For the geophysical application described in Kerr & Lister 1987 it is necessary to replace the rigid boundary condition (2.26*d*) by the free-slip condition $\partial u_-/\partial z = 0$. This simply changes the factor 4 in (2.28) to 3.)

The appropriate similarity solution to (2.28) subject to the usual volume constraint (2.10) is given by

$$\frac{\alpha-1}{3}H-\frac{2\alpha+1}{6}\eta H'=\frac{1}{\eta}(\eta H^2H')', \tag{2.29}$$

where

$$\eta=\eta_{\mathrm{N}}^{-1}\left(\frac{g'\rho_0 d}{4\mu_-}\right)^{-\frac{1}{6}}\left(\frac{Q}{2\pi}\right)^{-\frac{1}{3}}rt^{-(2\alpha+1)/6}, \tag{2.30a}$$

$$h(r,t)=\eta_{\mathrm{N}}\left(\frac{g'\rho_0 d}{4\mu_-}\right)^{-\frac{1}{3}}\left(\frac{Q}{2\pi}\right)^{\frac{1}{3}}t^{(\alpha-1)/3}H(\eta), \tag{2.30b}$$

and

$$\eta_{\mathrm{N}}=\left(\int_0^1 H\eta\,\mathrm{d}\eta\right)^{-\frac{1}{3}}. \tag{2.30c}$$

Using the boundary condition $H(1)=0$, we find that around $\eta=1$ the solution to (2.29) must satisfy

$$H\sim\left[\tfrac{1}{3}(2\alpha+1)(1-\eta)\right]^{\frac{1}{2}}\left[1-\frac{1}{4}\frac{1-2\alpha}{1+2\alpha}(1-\eta)+O(1-\eta)^2\right]. \tag{2.31}$$

This asymptotic result may be used as a starting condition for inwards numerical integration of (2.29). Some solutions of (2.29) are shown in figure 4(*a*) together with the approximations given by (2.31). The approximate solutions agree quite well with the true solutions except near $\eta=0$, where the true solutions have a singularity ($\alpha\neq 0$) due to the continual introduction of fluid. A graph of η_{N}, as a function of α is given in figure 4(*b*). It should be recalled that the modelling equations will only be valid at large times if $\alpha\leqslant 1$; if $\alpha>1$ the depth of intruding fluid increases with time and $h\ll d$ ceases to hold.

When $\alpha=0$, (2.29) and (2.30*c*) have the exact solutions

$$H=\left(\frac{1-\eta^2}{6}\right)^{\frac{1}{2}},\qquad \eta_{\mathrm{N}}=(54)^{\frac{1}{6}}. \tag{2.32a, b}$$

These results not only describe the interesting case of fixed volume release, but also provide a useful check on the accuracy of any numerical scheme for general solution of (2.29).

A two-dimensional current, spreading symmetrically in $-x_{\mathrm{N}}\leqslant x\leqslant x_{\mathrm{N}}$ over a shallow layer of depth d, may be analysed in a very similar way. The arguments leading to the expression (2.27) for the velocity in the lower layer carry through to the two-dimensional geometry. Local and global conservation of intruding fluid lead to

$$\frac{\partial h}{\partial t}=\frac{g'\rho_0 d}{4\mu_-}\frac{\partial}{\partial x}\left(h^2\frac{\partial h}{\partial x}\right),\quad \int_0^{x_{\mathrm{N}}}h\,\mathrm{d}x=Qt^{\alpha}. \tag{2.33a, b}$$

Use of the similarity variables

$$\xi=\xi_{\mathrm{N}}^{-1}\left(\frac{g'\rho_0 d}{4\mu_-}\right)^{-\frac{1}{4}}Q^{-\frac{1}{2}}xt^{-(2\alpha+1)/4}, \tag{2.34a}$$

$$h(x,t)=\xi_{\mathrm{N}}\left(\frac{g'\rho_0 d}{4\mu_-}\right)^{-\frac{1}{4}}Q^{\frac{1}{2}}t^{(2\alpha-1)/4}H(\xi), \tag{2.34b}$$

$$\xi_{\mathrm{N}}=\left(\int_0^1 H\,\mathrm{d}\xi\right)^{-\frac{1}{2}} \tag{2.34c}$$

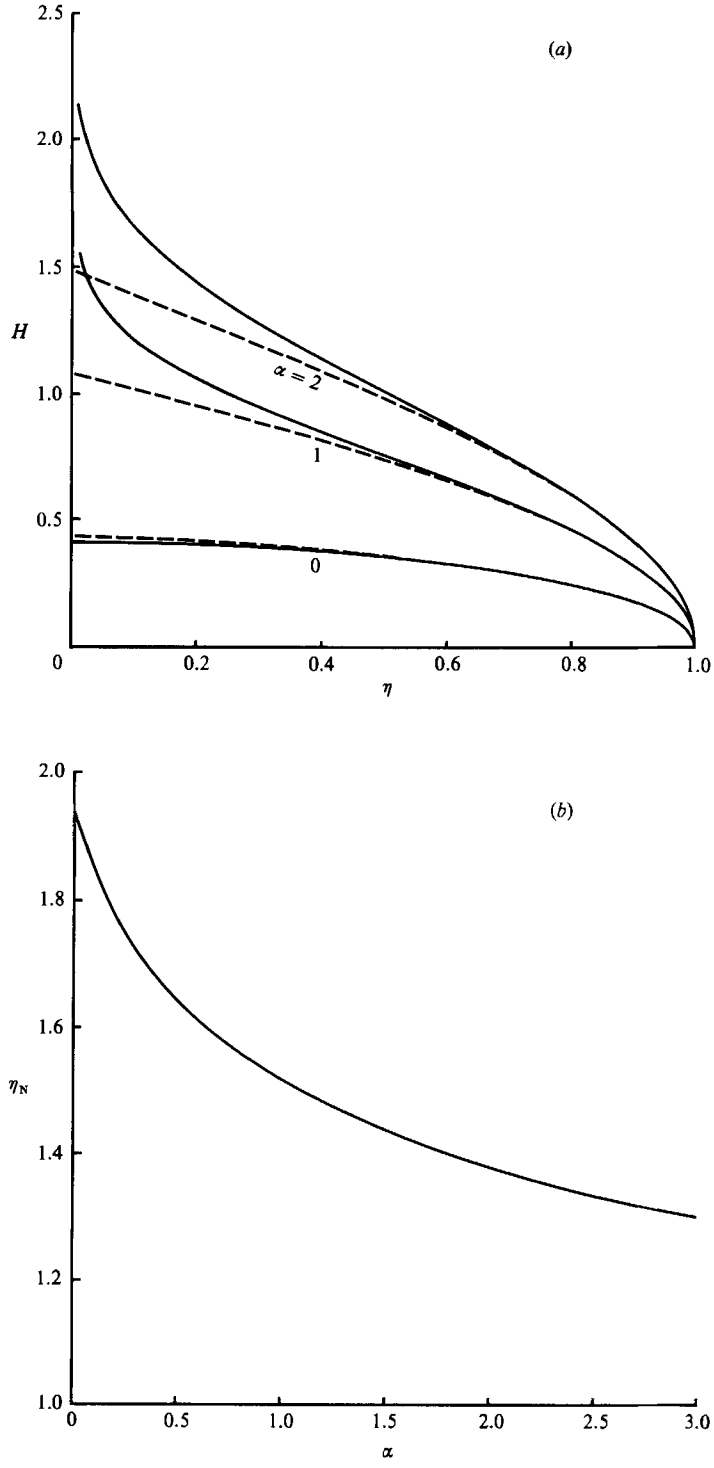

FIGURE 4. An axisymmetric gravity current, of volume Qt^{α}, spreading over a shallow layer of viscous fluid. (*a*) The shape of the current; true solutions are shown solid; the asymptotic approximations (2.31) are shown dashed; (*b*) the dimensionless length η_N of the current as a function of α.

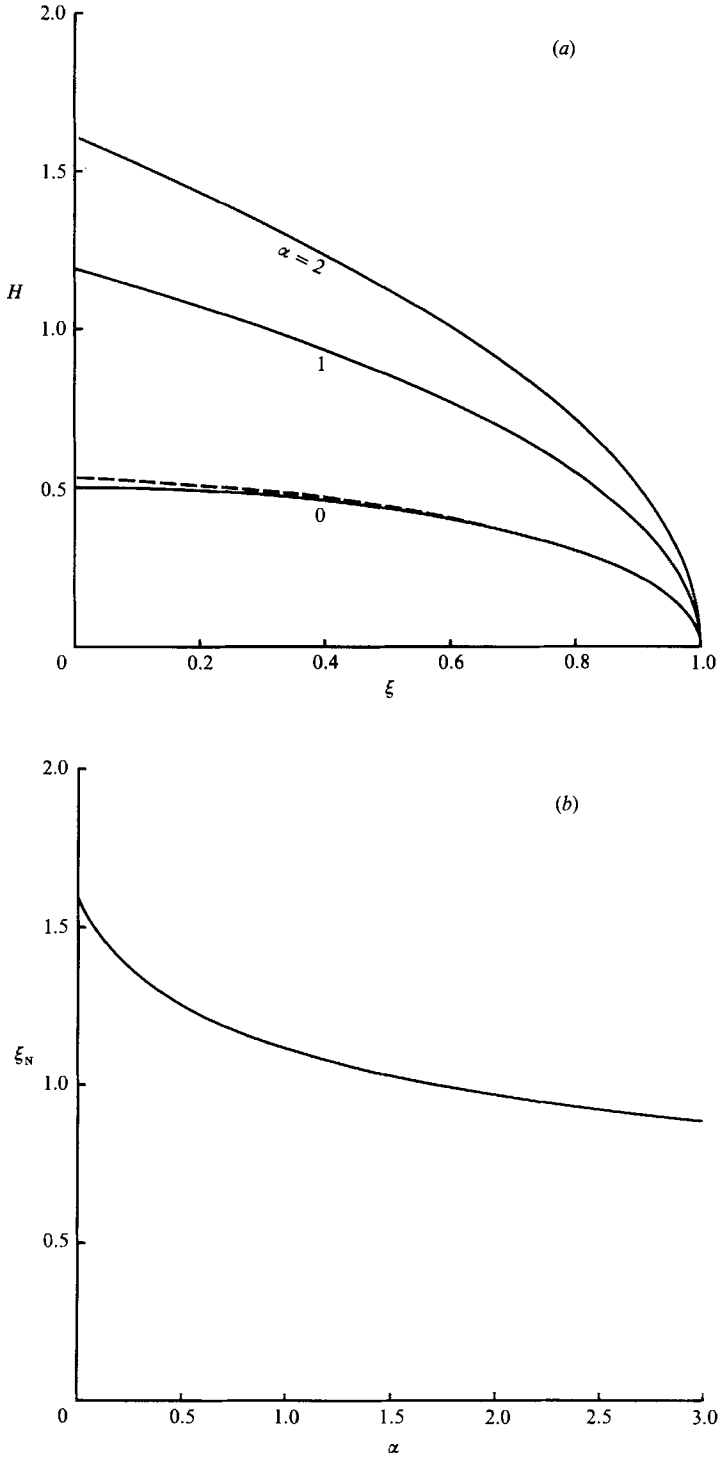

FIGURE 5. A two-dimensional gravity current, of volume Qt^α, spreading over a shallow layer of viscous fluid. (*a*) The shape of the current; true solutions are shown solid; the asymptotic approximation (2.35) is shown dashed for $\alpha = 0$ and is indistinguishable from the true solution for $\alpha = 1, 2$; (*b*) the dimensionless length ξ_N of the current as a function of α.

gives rise to
$$\frac{2\alpha-1}{4}H-\frac{2\alpha+1}{4}\xi H' = (H^2H')' \tag{2.35}$$

with local solution
$$H \sim [\tfrac{1}{2}(2\alpha+1)(1-\xi)]^{\frac{1}{2}}\left[1-\frac{1}{12}\frac{3-2\alpha}{1+2\alpha}(1-\xi)+O(1-\xi)^2\right]. \tag{2.36}$$

Numerical and asymptotic solutions for H are shown in figure 5(*a*); the dependence of the constant ξ_N on α is shown in figure 5(*b*).

Once again, we can obtain an exact solution for fixed volume release ($\alpha = 0$):
$$H = \frac{(1-\xi^2)^{\frac{1}{2}}}{2}, \qquad \xi_N = \left(\frac{8}{\pi}\right)^{\frac{1}{2}}. \tag{2.37a, b}$$

A further analytic solution may be obtained for the case $\alpha = \frac{3}{2}$:
$$H = (2(1-\xi))^{\frac{1}{2}}, \qquad \xi_N = \left(\frac{9}{8}\right)^{\frac{1}{4}}. \tag{2.38a, b}$$

3. Experiments

In the previous section explicit formulae were derived for the spread of a viscous intrusion into deep fluid and over a shallow layer of fluid. We now describe experiments conducted to verify these formulae.

The ambient fluid in the majority of our experiments was a glucose syrup (manufactured under the trademark 'Globe'). At room temperature this syrup has a specific gravity of about 1.43 and a kinematic viscosity in the range 400–750 cm^2 s^{-1}. The intruding fluids in these experiments were solutions of 25–30 wt. % glycerol (S.G. 1.26) and about 1 wt. % water in another glucose syrup of greater mean molecular weight and hence much greater viscosity ($\nu \approx 10^5$ cm^2 s^{-1}). It was therefore possible to prepare an intruding fluid of given viscosity and density by varying the ratios syrup to glycerol and syrup to water independently. A few preliminary experiments, to be described briefly later, used other combinations of fluids: one used solutions of 1,1,2-trichloro-1,2,2-trifluoroethane (S.G. 1.58) in polybutenes (S.G about 0.88, manufactured under the trademark 'Hyvis') of appropriate molecular masses and viscosities; the remainder used solutions consisting of about 80 wt. % glycerol (S.G. 1.26) and about 20 wt. % aqueous potassium carbonate solution (S.G. 1.00–1.54, depending on concentration). In each of these systems the ambient and intruding fluids were miscible and the intruding fluid was dyed to aid visualization.

The viscosities of binary glycerol–water mixtures were calculated from measurements of refractive index using tables in Miner & Dalton (1953). The viscosities of all the other fluids were measured over a range of temperatures using a U-tube viscometer and densities were measured using a hydrometer. All of these measurements were accurate to within 1 %, though, in practice, variations in temperature across the experimental tank and during the course of the experiments increased the uncertainty in the viscosity to typically 5 %. Measurements of the extent of the current were made both by eye and from video recordings using either a rule laid across the tank or millimetre-ruled graph paper placed under the tank. Parallax errors were calibrated and eliminated to within 1 %.

Five geometries and the corresponding spreading laws were investigated in a series of experiments using glucose syrups. In each case the gravity current consisted of a

light intruding syrup spreading over the free surface of a denser ambient syrup. As a precaution, prior to each experiment the free surface of the ambient syrup was scraped to remove any air-borne dust that had settled, and the apparatus was then covered for the duration of the experiment. The necessity for this precaution is discussed later. The apparatus and method of release in each geometry are detailed below and summarized in table 1(*a*). The other experimental parameters are summarized in table 1(*b*).

(i) *Experiments 1–3.* Three experiments were conducted to investigate fixed volume, axisymmetric spread over a shallow layer. In each experiment the shallow layer was contained in a circular flat-bottomed Perspex tank of internal diameter 90 cm that had previously been levelled to within 0.3 mm. The layer depths away from the sidewall meniscus were in the range 5–8.5 cm. Buoyant fluid was initially confined at the centre of the tank within a Perspex cylinder; the internal diameters of the cylinders used were 13.5, 24 and 14.5 cm respectively. At the start of each experiment the cylinder was raised, producing an axisymmetric gravity current. The volumes of buoyant fluid used in the calculation of results take account of the amount of fluid adhering to the barrier on release.

(ii) *Experiments 4–6.* Three further experiments were conducted in the circular tank described above. In these experiments buoyant fluid was continually released at the centre of the tank from a pipe draining a reservoir of the fluid. A nearly constant flux was achieved by maintaining the head of the reservoir to within 3%. The orifice of the pipe was clamped about 1 cm above the fluid level in the tank and the inertia of the fluid issuing from the pipe was negligible.

(iii) *Experiment 7.* Our final investigation of flow over a shallow layer considered two-dimensional fixed volume release. A flat-bottomed Perspex tray, 50 cm square, was filled to a depth of nearly 5 cm with the ambient fluid. The buoyant fluid was released from behind a straight barrier, parallel to, and several centimetres from, the endwall of the tray. A nearly two-dimensional current was produced with the effects of the finite span of the current apparently restricted to a retardation within 5 cm of the sidewalls; variations across the central 40 cm of the current were negligible.

(iv) *Experiments 8 and 9.* These experiments investigated the axisymmetric spread of a fixed flux of buoyant fluid over a large volume of ambient fluid contained within a circular Perspex tank, 73 cm in internal diameter and filled to a nominal depth of 35 cm. The point of release of the buoyant fluid, at the centre of the tank, was thus about 35 cm from any of the tank's boundaries. As in Experiments 4–6, a nearly constant flux release was effected using a pipe and reservoir though in this case it was only possible to maintain the head to within 6%.

(v) *Experiments 10–12.* These three experiments are representative of a number of experiments, not reported here in detail, which involved axisymmetric spread of a fixed volume of fluid over a large volume of denser fluid. In Experiments 10 and 12 the buoyant fluid was released from within Perspex cylinders, of internal diameters 5 cm and 10 cm respectively, into ambient fluid of approximate depth 20 cm contained in a cylindrical vessel of internal diameter 40 cm. Experiment 11 was conducted in the 73 cm internal diameter tank described above. The intruding fluid was added through a wide funnel during the first 30 s of the experiment, the circular nozzle of the funnel ensuring that the initial conditions were axisymmetric.

(vi) *Experiment 13.* The results of the three experiments just described should be compared with the results from an early trial experimental using polybutenes, which considered the spread of an axisymmetric current between two deep layers of fluid. The intruding fluid was injected from a calibrated syringe, through an attached

(*a*)

Expts	Ambient fluid	Geometry	Buoyant fluid
1–3	Shallow	Axisymmetric	Fixed volume
4–6	Shallow	Axisymmetric	Fixed flux
7	Shallow	Two-dimensional	Fixed volume
8–9	Deep	Axisymmetric	Fixed flux
10–13	Deep	Axisymmetric	Fixed volume

(*b*)

Expt	ρ_- (g cm^{-3})	ρ_0 (g cm^{-3})	ρ_+ (g cm^{-3})	g' (cm s^{-2})	ν_- (cm^2 s^{-1})	ν_0 (cm^2 s^{-1})	ν_+ (cm^2 s^{-1})	Q	d (cm)
1	1.429	1.394	—	24	720	670	—	1023 cm^3	8.1
2	1.429	1.394	—	24	720	670	—	933 cm^3	7.2
3	1.429	1.399	—	21	690	740	—	252 cm^3	5.15
4	1.429	1.3955	—	23	700	760	—	0.243 cm^3 s^{-1}	7.7
5	1.429	1.397	—	22	730	620	—	0.278 cm^3 s^{-1}	6.6
6	1.429	1.399	—	24	625	620	—	0.0126 cm^3 s^{-1}	4.6
7	1.428	1.3935	—	24	450	330	—	15.4 cm^2	4.75
8	1.4285	1.391	—	26	650	590	—	0.244 cm^3 s^{-1}	—
9	1.4285	1.3935	—	24	460	330	—	0.401 cm^3 s^{-1}	—
10	1.429	1.403	—	18	880	1100	—	33.7 cm^3	—
11	1.4285	1.391	—	26	610	550	—	242 cm^3	—
12	1.429	1.403	—	18	720	800	—	478 cm^3	—
13	0.895	0.887	0.8805	4.0	62	58	55	5.0 cm^3	—

TABLE 1. (*a*) The experimental geometries; (*b*) the experimental parameters

nozzle, at the interface of a two-layer stratified system. The layers were contained in a cylindrical glass vessel of internal diameter 17 cm and had depths of nominally 8 cm. The vessel was placed on a millimetre ruled sheet of paper and was covered by a Perspex sheet on which was marked an identical millimetre grid. Corresponding marks on the sheet of paper and on the cover were lined up to avoid parallax errors in the measurement of the radius of the spreading intrusion. Though this was a small-scale experiment, it is of some interest because it involved spread at an internal density interface and not at an air–fluid free surface.

The results of these thirteen experiments are shown in figure 6(*a–e*) together with the theoretical predictions derived in §2,

$$r_N = 0.836\left(\frac{\rho_0 Q^2 g' d}{\mu_-}\right)^{\frac{1}{6}} t^{\frac{1}{6}} \quad \text{(Expts 1–3)}, \tag{3.1a}$$

$$r_N = 0.653\left(\frac{\rho_0 Q^2 g' d}{\mu_-}\right)^{\frac{1}{6}} t^{\frac{1}{2}} \quad \text{(Expts 4–6)}, \tag{3.1b}$$

$$x_N = 1.128\left(\frac{\rho_0 Q^2 g' d}{\mu_-}\right)^{\frac{1}{4}} t^{\frac{1}{4}} \quad \text{(Expt 7)}, \tag{3.1c}$$

$$r_N = 0.309\left(\frac{\rho_0 Q^2 g'}{\mu_-}\right)^{\frac{1}{5}} t^{\frac{3}{5}} \quad \text{(Expts 8, 9)}, \tag{3.1d}$$

and

$$r_N = 0.689\left(\frac{\rho_0 Q^2 g'}{\mu_- + \mu_+}\right)^{\frac{1}{5}} t^{\frac{1}{5}} \quad \text{(Expts 10–13)}. \tag{3.1e}$$

In each case the extent of the current is drawn scaled by the appropriate (dimensional) coefficient of t from (3.1) in order to allow data from each group of experiments to collapse onto a single curve.

The asymptotic agreement between theory and experiment as $t \to \infty$ in each of the four geometries represented by (3.1*a–d*) is good. In three of these geometries several experiments with differing parameters were conducted and the theoretical scaling of the results is confirmed by a successful collapse of the data. It should be noted that the theoretical solution describes the large-time experimental behaviour; at early times the experimental intrusions did not satisfy the geometrical constraints, such as $H \ll L$, required for the theoretical solutions to be valid. This point also explains the closer agreement at early times of the fixed flux releases (Expts 4–6, 8, 9) compared with the fixed volume releases (Expts 1–3, 7). In the latter experiments, in order to have sufficient depths of buoyant fluid at large times for the intrusion to be observable, the depth of buoyant fluid at early times had to be a significant fraction of the total depth of the fluid layer, whereas in the constant-flux experiments the intrusion thickness is nearly constant in time (equations (2.30*b*) and (2.11*b*)) and was observed to be in the range 3–8 mm, much less than the layer depth.

An indication of the shapes of the intrusions at early times may be found in figures 7 and 8 which show side views of Experiments 1 and 4. Each photograph is such that, at the distance from the camera of the intrusion, the depth of the fluid layer fills the frame, with the upper edge of the frame coinciding with the free surface and the lower edge with the base of the tank. The angle at which the nose of the intrusion appears to meet the free surface may be influenced by optical effects at the air–fluid interface. In connection with our earlier remarks, we note that the fixed-volume intrusion shown in figure 7 was initially flat-bottomed and occupied some 80 % of the fluid

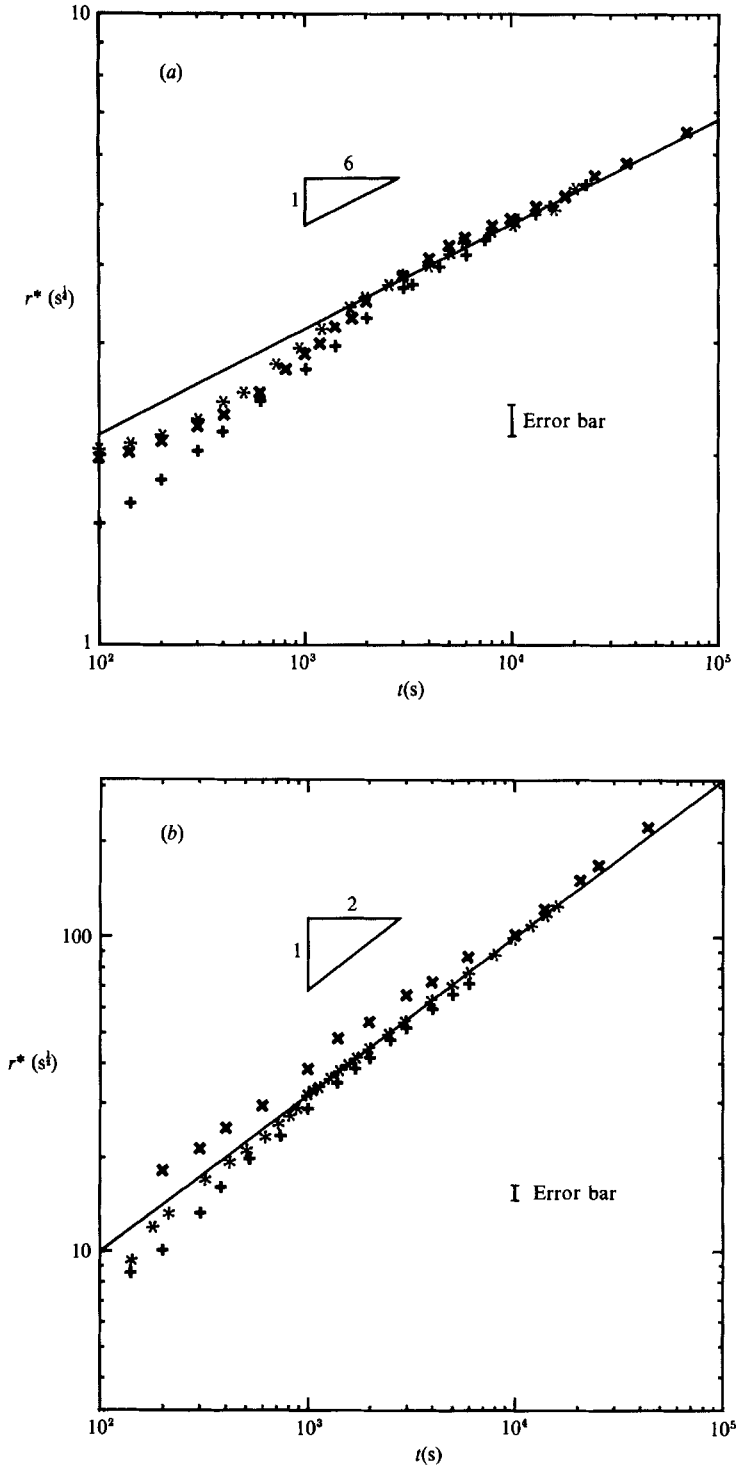

FIGURE 6(a, b). For caption see page 233.

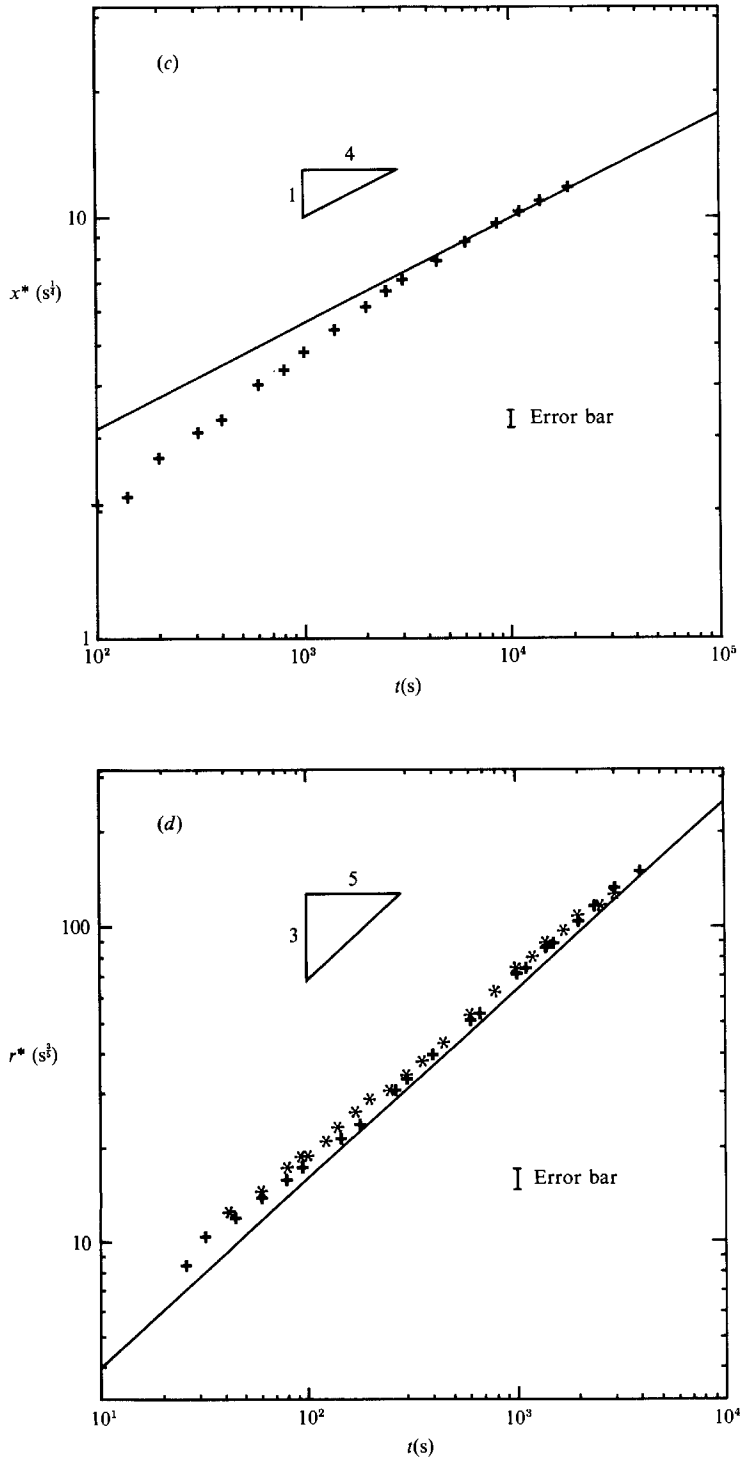

FIGURE 6 (*c*, *d*). For caption see facing page.

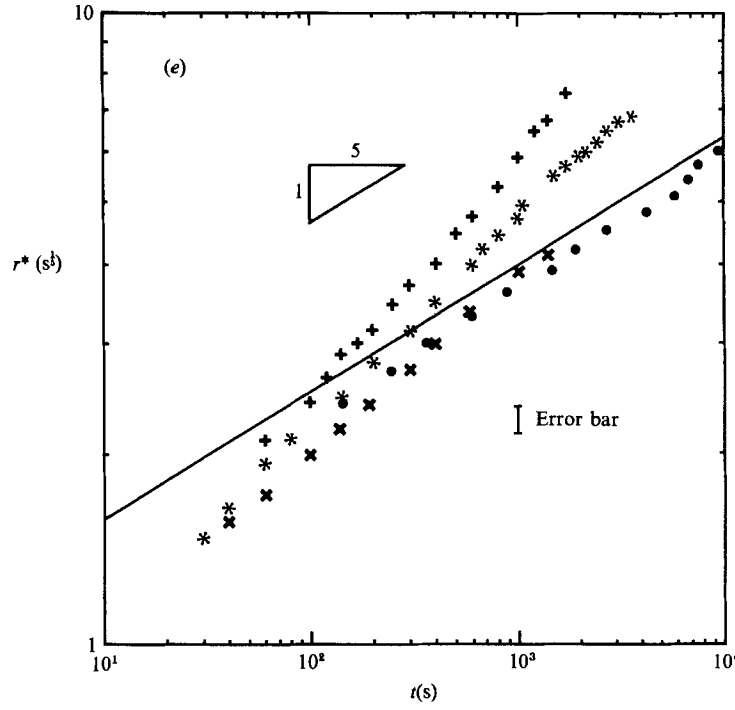

FIGURE 6. (*a*) Experimental values of $r^* = r(27\rho_0 Q^2 g' d/8\pi^2\mu_-)^{-\frac{1}{6}}$ as a function of time for the axisymmetric spreading of a constant volume of syrup over a shallow ambient layer. (+, Expt 1; *, Expt 2; ×, Expt 3; theoretical solution shown as solid line.) (*b*) Experimental values of $r^* = (r/0.653)(\rho_0 Q^2 g' d/\mu_-)^{-\frac{1}{6}}$ as a function of time for the axisymmetric spreading of a constant flux of syrup over a shallow ambient layer. (+, Expt 4; *, Expt 5; ×, Expt 6; theoretical solution shown as solid line.) (*c*) Experimental values of $x^* = x(16\rho_0 Q^2 g' d/\pi^2\mu_-)^{-\frac{1}{4}}$ as a function of time for the two-dimensional spreading of a constant volume of syrup over a shallow ambient layer. (+, Expt 7; theoretical solution shown as solid line.) (*d*) Experimental values of $r^* = (r/0.309)(\rho_0 Q^2 g'/\mu_-)^{-\frac{1}{5}}$ as a function of time for the axisymmetric spreading of a constant flux of syrup over a deep ambient layer. (+, Expt 8; *, Expt 9; theoretical solution shown as solid line.) (*e*) Experimental values of $r^* = r(125\rho_0 Q^2 g'/256\pi(\mu_- + \mu_+))^{-\frac{1}{5}}$ as a function of time for the axisymmetric spreading of a constant volume of syrup or of polybutene between deep ambient layers. (+, Expt 10; *, Expt 11; ×, Expt 12; ●, Expt 13; theoretical solution shown as solid line.)

depth. The spread of the intrusion was retarded for some time by the resistance to ambient fluid flowing to fill the relatively thin gap under the buoyant fluid as the gap widened. In contrast, the fixed-flux intrusion shown in figure 8 was much thinner and, even near the central bulge under the point of supply, occupied a small fraction of the layer depth.

After the good asymptotic agreement between theory and experiment in the four geometries investigated in Experiments 1–9, the poor agreement in the remaining geometry – fixed volume, axisymmetric spread over deep fluid – is puzzling. In Experiments 10–12 the dependence on t appears to be more rapid than $t^{\frac{1}{5}}$; in Experiment 13 the dependence on t is close to $t^{\frac{1}{5}}$ but with a smaller coefficient than expected. Among the experiments conducted in this geometry using syrups as the experimental fluids, there is some evidence of an improvement in the results with an increase in Q. These points are discussed more fully in the following section.

To close this section, it is worthwhile to note the necessity of maintaining a dust-free surface on the ambient fluid. In a series of preliminary experiments using

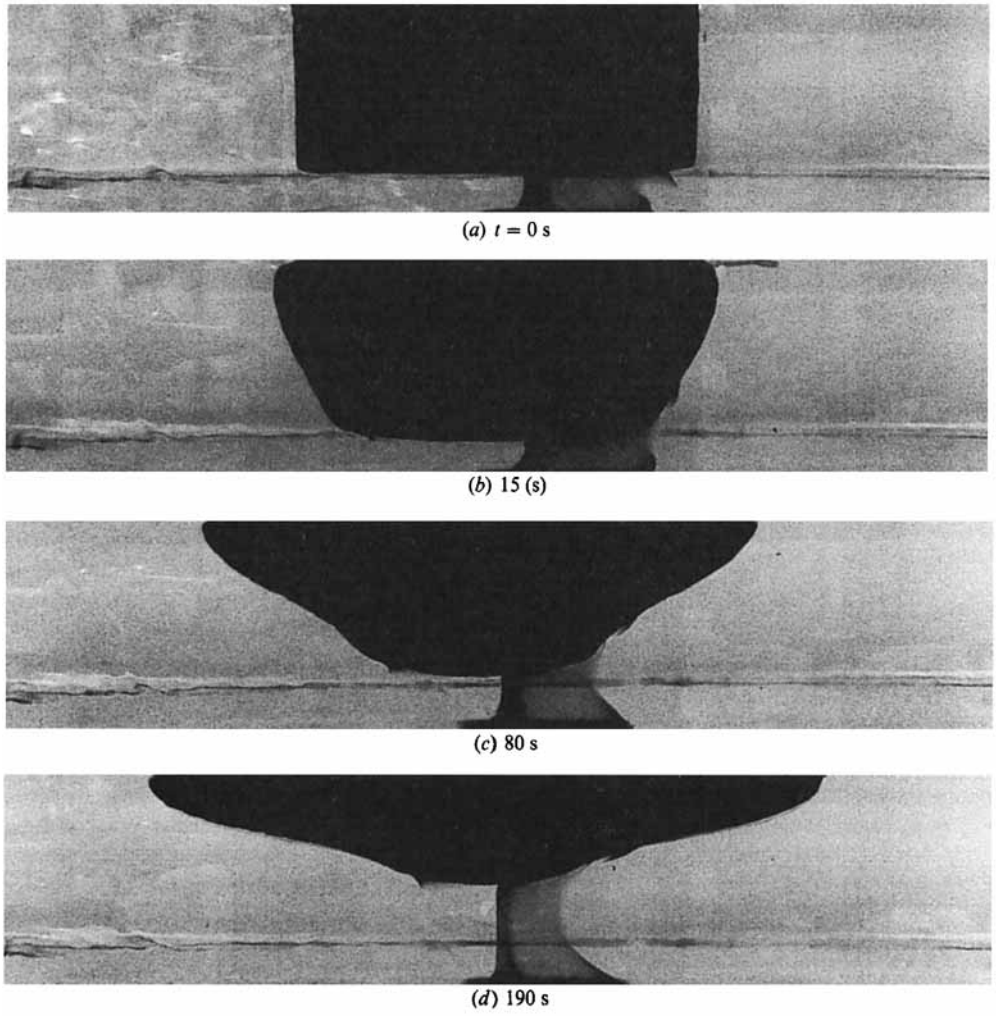

FIGURE 7. Side views of the spread of an axisymmetric gravity current containing a fixed volume of buoyant, dyed syrup (Experiment 1, parameters given in table 1*b*). The first frame was taken before the release of the buoyant fluid from within a cylindrical Perspex barrier of internal diameter 14.5 cm. The depth of the fluid layer was 8.1 cm and fills each frame at the distance of the current. It should be noted that the shape of the buoyant fluid remains flat-bottomed for some time, owing to the large resistance to the inward flow of denser fluid beneath the spreading current. (The horizontal line near the bottom of each frame is the back edge of the tank; optical effects may influence the apparent angle at which the nose of the intrusion meets the free surface.)

uncovered glycerol solutions we observed that the leading edge of the current showed radial striations, visible some distance towards the source of the intrusion. An example of these striations is reproduced in figure 9. Increasing contamination of the fluids by atmospheric dust was reflected by an increasing intensity of the striated pattern and greater departures from (3.1) towards the slower spread associated with flow over a rigid surface. The striations are very similar to those reported as occurring in other 'free-surface' flows (Britter & Simpson 1978; Huppert & Simpson 1980; Didden & Maxworthy 1982) and are attributable to surface contamination of

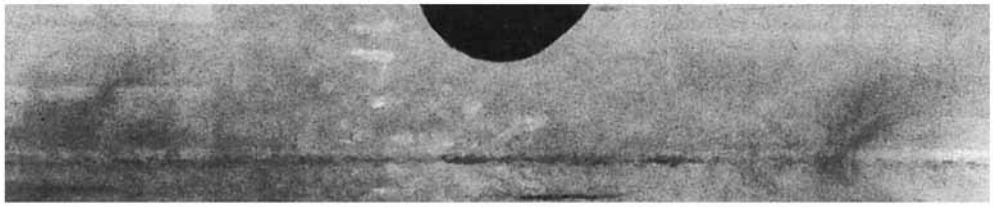

(*a*) $t = 200$ s

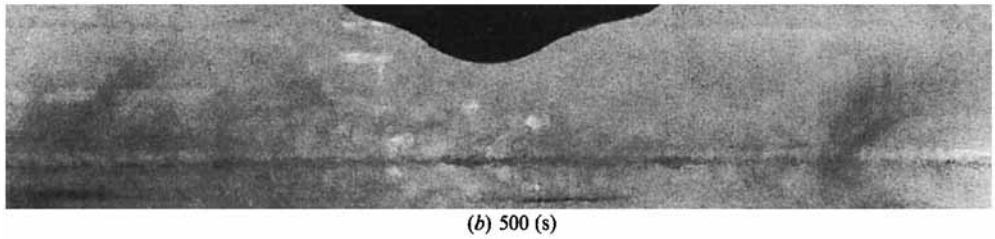

(*b*) 500 (s)

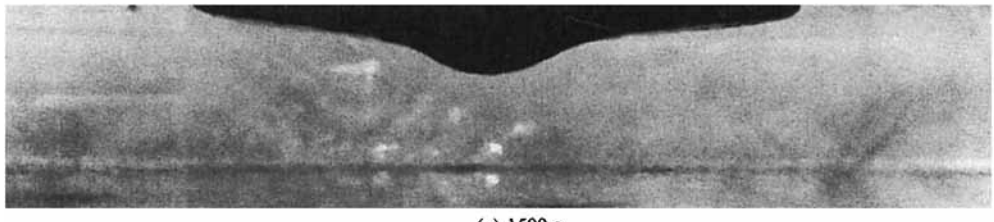

(*c*) 1500 s

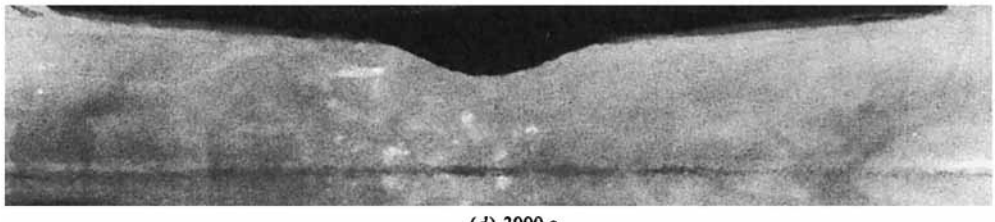

(*d*) 3000 s

FIGURE 8. Side views of the axisymmetric spread of a gravity current fed by a fixed flux of buoyant fluid at its centre (Experiment 4, parameters given in table 1*b*). The total fluid depth was 7.7 cm and, even near the centre of the current, the thickness of the spreading current was much less than this. The average thickness of the current was about 5.5 mm, except just after the start of the experiment.

the glycerol which causes the air–glycerol interface to act as a rigid rather than as a free surface. Ambient fluid, at rest next to the rigid surface by virtue of the 'no-slip' condition, is consequently under-run by the spreading intrusion. This overlay of a less dense fluid by a more dense fluid causes gravitational instability and the striated pattern. In Experiments 1–12, the scraping of the surface of the ambient fluid, described earlier, successfully removed contaminants from the fluid surface and no evidence of striations or of rigidity in the free surface was observed.

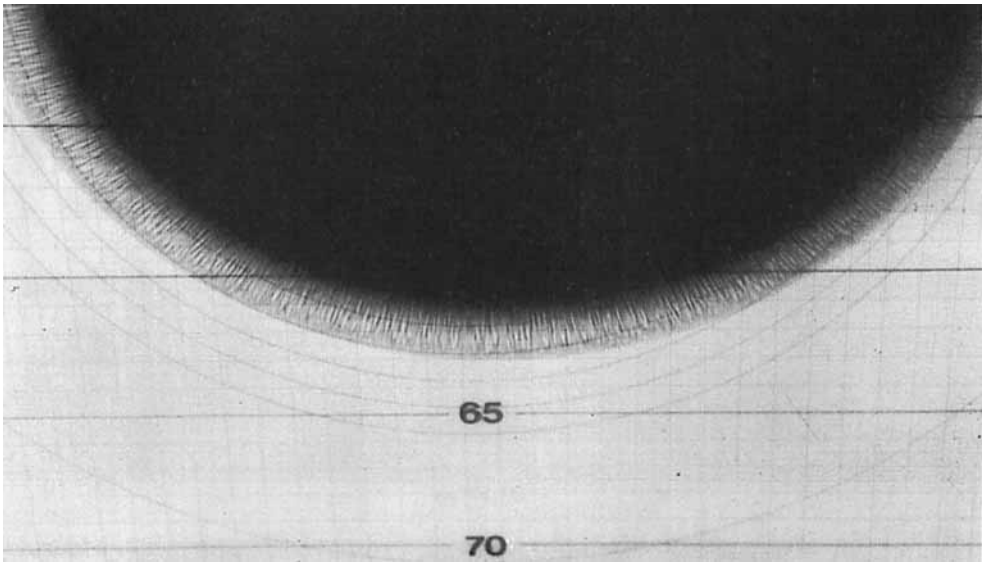

FIGURE 9. In a series of preliminary experiments involving glycerol solutions, the leading edge of the intrusion developed a radially striated pattern. This pattern is caused by contamination of the fluid surface by dust. The example shown occurs on the edge of an axisymmetric current containing 19.0 cm^3 of glycerol solution, dyed blue, density 1.227 g cm^{-3} and viscosity 1.10 $cm^2\ s^{-1}$, which is spreading over a 2.6 cm deep layer of another glycerol solution, density 1.349 g cm^{-3} and viscosity 1.15 $cm^2\ s^{-1}$. The photograph was taken approximately 100 min after release and the scale is in cm. The fuzzy appearance of the edge of the current is due to the striations.

4. Discussion

The spread of axisymmetric and two-dimensional intrusions along a fluid interface has been investigated theoretically and experimentally. In two cases, intrusion between deep layers of viscous fluid and flow over a shallow layer, complete analytic solutions of the equations of motion have been found in similarity form. These solutions give both the shape of the intrusion and the scaling and numerical coefficient in the spreading law. The scaling of the results and the time-dependence of the flows are also derived independently in an Appendix using the simple but powerful technique of scaling analysis.

The analytic results can be compared with the results of our experiments. For the experimental parameters used, the neglect of inertial forces (as assumed in the theory) was justified after at most a few seconds. Diffusion was also negligible on the timescale of our experiments. Five different spreading laws have been investigated. In four cases the experimental results and theoretical predictions are in good agreement, both with regard to the time-dependence of the extent of the current and with the scaling on the physical parameters of the current. The numerical coefficients are also in agreement to within experimental accuracy. Predictions in which $r \propto t^{\frac{3}{5}}$, $r \propto t^{\frac{1}{2}}$, $r \propto t^{\frac{1}{4}}$, and $r \propto t^{\frac{1}{6}}$ have each been verified in the appropriate geometry. The results from axisymmetric spread of a fixed volume over deep fluid are disappointing and merit discussion.

The first point to make is that, as derived in Appendix A, the $t^{\frac{1}{5}}$ time-dependence and the scaling on the physical parameters (Q, g' and μ_-) of the theoretical prediction

are given by simple scaling estimates, (A 3) and (A 4), of the buoyancy force and viscous resistance. The same estimates are used successfully in the Appendix to predict the rate of spread in the four other geometries. Further, we note that the same analysis that gave the numerical coefficient in (3.1*e*) from solution of (2.12), also led to the theoretical prediction (3.1*d*) for fixed flux release which does agree with experiment. An algebraic error in the theory seems unlikely, therefore, and we conclude that the experiments were affected by a physical process other than the simple balance of viscous and buoyancy forces modelled. The presence of the walls of the experimental tank would reduce the flow in the ambient fluid and slow the spread of the current and, hence, cannot explain the results of Experiments 10–12 in which the spread was faster than expected. The finite size of the apparatus is, however, the most likely explanation for the slower spread in Experiment 13. As noted earlier, inertial effects were completely negligible owing to the large viscosities of the fluids (see (A 9) in Appendix A).

Two possible candidates for an effect that could increase the rate of spread of a gravity current are thermal convection in the ambient fluid and gradients of surface tension in the free surface. Since the spreading currents were observed to remain very nearly circular, an explanation in terms of thermal convection would require toroidal convection in the ambient fluid driven by sidewall cooling. However, background convection currents observed by means of floating tracer particles were neither axisymmetric nor large enough to explain the experimental discrepancies. A more likely mechanism is augmentation of the buoyancy forces by gradients in the air–fluid surface tension caused by the differing compositions of the syrups. The phenomenon is the same as observed when the surface of a pool of water is 'pulled apart' when a drop of detergent is placed on it. This hypothesis explains why Experiment 13 gave dissimilar results to Experiments 10–12, since the former intrusion took place between miscible fluids and not at an air–fluid interface. As the ratio of buoyancy forces to interfacial forces increases with volume, this hypothesis also gives some explanation for the improvement in the results with the volume of buoyant fluid and for the good results in other geometries, in which larger volumes of fluid were, in general, used. However, it is surprising that the other geometries show no evidence of spreading driven by surface tension.

Returning to the theoretical models, in Appendix A §A.1 it is shown that if α is less than a critical value α_1 then an intrusion between deep layers will initially propagate under an inertial–buoyancy balance, but will ultimately propagate under a viscous–buoyancy balance. Here $\alpha_1 = \frac{1}{4}$ for a two-dimensional current and $\alpha_1 = \frac{3}{4}$ for an axisymmetric current. Our analysis will be valid for times much greater than the transition time between the regimes, a time which is estimated in Appendix A §A.1. If, however, $\alpha > \alpha_1$ then an initial viscous–buoyancy balance will give way to a regime in which inertia is important and our analysis breaks down. In this inertial regime the Stokes flow in the ambient fluid is replaced by a viscous boundary layer. Arguments are given in the Appendix showing that this leads to spreading laws of the form $r \propto t^{(4\alpha+3)/8}$ (two-dimensional) and $r \propto t^{(4\alpha+3)/12}$ (axisymmetric), valid at large times provided $\alpha > \alpha_1$.

Our analysis of flow over a shallow layer was made under the assumption that the thickness of the intrusion was much less than that of the layer. This will ultimately be the case if $\alpha < \alpha_2$, where $\alpha_2 = \frac{1}{2}$ for a two-dimensional current and $\alpha_2 = 1$ for an axisymmetric current. If $\alpha > \alpha_2$ then the intrusion thickens with time and violates the assumption.

If the fluids are miscible then diffusion will eventually become important when the

diffusive boundary layer becomes much thicker than the intrusion. Spreading relations for diffusion-dominated intrusions are given in Appendix A §A.2.

Finally, we note that the analytic solutions presented in §2 describe the spreading regimes that were relevant to the geophysical application analysed in Kerr & Lister (1987). Many of the other spreading regimes identified in Appendix A have not yet received a theoretical treatment and might give rise to analytic solutions. Experiments should be performed to verify the consequent theoretical predictions.

We would like to thank Corn Products Co., Manchester for their donation of the considerable quantities of glucose syrups used in our experiments. Constructive comments from H. E. Huppert and M. G. Worster are gratefully acknowledged. Our research was supported by the Natural Environment Research Council (J. R. L.) and by the Royal Commission for the Exhibition of 1851, and Churchill College, Cambridge (R. C. K).

Appendix A. Scaling analysis

The rate of spread of a viscous intrusion can be found by equating estimates of the buoyancy forces driving the motion and of the viscous drag exerted by the ambient fluid on the intruding fluid. As indicated below, this approach is similar to that used in some particular geometries by a number of authors. The scaling analysis presented here highlights the physical balances underlying viscous gravity currents and provides an understanding of a wide variety of intrusive situations. We consider both two-dimensional and axisymmetric currents occurring along an interface, or at a free surface, or along a horizontal rigid boundary.

Let the typical vertical and horizontal extent of the current be H and $L\,(\gg H)$ respectively, and suppose the total volume of intruding fluid is Qt^{α}, where α and Q are positive constants. For brevity, we shall treat the two-dimensional and axisymmetric cases together. Thus

$$HL^{n+1} \sim Qt^{\alpha}, \tag{A 1}$$

where $n = 0$ for a two-dimensional current and $n = 1$ for an axisymmetric current. Let D be the vertical scale of motion in the ambient fluid and U be a typical horizontal velocity within the intrusion. Then

$$U \sim \frac{L}{t}, \tag{A 2}$$

the total buoyancy force is given by

$$F_{\mathrm{g}} \sim \rho g' H^2 L^n \sim \frac{\rho g' Q^2}{L^{n+2}} t^{2\alpha}, \tag{A 3}$$

and the viscous drag exerted by the ambient fluid on the intrusion is given by

$$F_{\mathrm{v}} \sim \frac{\mu U L^{n+1}}{D} \sim \frac{\mu L^{n+2}}{Dt}. \tag{A 4}$$

A.1. *The effects of geometry*

We neglect the effects of diffusion and surface tension. Once D is specified, then, by equating the right-hand sides of (A 3) and (A 4), we can determine the spreading law for the intrusion. We consider below four cases of currents spreading under a balance between viscous and buoyancy forces.

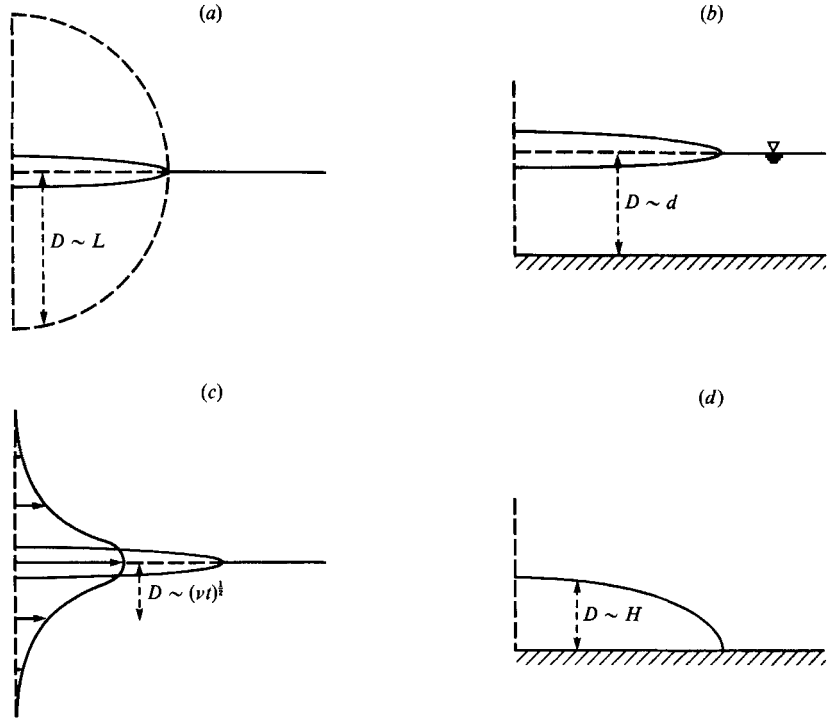

FIGURE 10. The spread of a viscous intrusion: (*a*) between deep layers of fluid in Stokes flow (region of influence shown dashed); (*b*) over a layer of shallow depth d; (*c*) resisted by a viscous boundary layer; and (*d*) over a rigid surface.

(*a*) Suppose the intrusion takes place far from rigid boundaries into a large volume of viscous fluid (figure 10*a*). Assume also that the intrusion is sufficiently sluggish that inertia may be neglected. The ambient fluid will thus be in Stokes flow driven by the buoyancy of the intrusion. This flow will be equidimensional and so $D \sim L$. Hence

$$L \sim \left(\frac{g'Q^2}{\nu}\right)^{1/(2n+3)} t^{(2\alpha+1)/(2n+3)}. \tag{A 5}$$

(*b*) Alternatively, suppose the intrusion consists of a current along the surface of a shallow layer of viscous fluid (figure 10*b*). Suppose too that the layer has a constant depth d and that $H \ll d \ll L$. Then $D \sim d$ and

$$L \sim \left(\frac{g'Q^2 d}{\nu}\right)^{1/(2n+4)} t^{(2\alpha+1)/(2n+4)}. \tag{A 6}$$

(*c*) The third case we consider is that in which the intrusion takes place into a relatively inviscid environment. The adjustment between slug flow in the viscous intruding fluid and zero velocity at distance into the ambient fluid is made in a thin boundary layer of thickness $D \sim (\nu t)^{\frac{1}{2}}$ (figure 10*c*). Thus

$$L \sim \left(\frac{g'^2Q^4}{\nu}\right)^{1/(4n+8)} t^{(4\alpha+3)/(4n+8)}. \tag{A 7}$$

The spreading laws (A 7) have been given previously only in the particular cases of $\alpha = 0$ (Fay 1969; Hoult 1972) and $\alpha = 1$ (Didden & Maxworthy 1982).

(*d*) Finally, when a viscous gravity current flows over a rigid surface (figure 10*d*) the shear is concentrated within the current itself. (We assume that H is much less than the vertical scale of the motion in the ambient fluid.) We must therefore replace D by H in (A 4) when calculating the viscous retarding force. When this is done we obtain

$$L \sim \left(\frac{g'Q^3}{\nu}\right)^{1/(3n+5)} t^{(3\alpha+1)/(3n+5)}, \tag{A 8}$$

where ν is now the viscosity of the intruding fluid (Huppert 1982; Maxworthy 1983).

Comparison between (A 5), (A 6), (A 7) and (A 8) shows clearly the importance of geometry in determining the rate of spread of a gravity current. The rate depends critically upon the vertical scale D of the viscous drag inhibiting spread. In more complicated geometries the drag may be concentrated in either the fluid above or below the intrusion and the situation can be reduced to one of the four simple cases above. For example, in an intrusion between a shallow layer of viscous fluid with a rigid boundary and a deep layer of viscous fluid, the drag exerted by the shallow layer dominates that exerted by Stokes flow in the deep layer. Therefore, provided that the intrusion is much thinner than the depth of the shallow layer, it will spread according to (A 6) and not (A 5). Further extensions of these ideas to include the effects of surface tension, diffusion and a stratified environment are described later in this Appendix.

We conclude this section with a discussion of the conditions necessary for the validity of (A 5)–(A 7). Similar constraints will apply to (A 8) but are described by Huppert (1982) and will be omitted here.

The models giving rise to (A 5) and (A 7) are in many senses complementary. If the ambient fluid is very viscous then it will be driven in Stokes flow and (A 5) will be valid; if it is relatively inviscid then it will contain a thin inertial boundary layer and (A 7) will hold. The distinction between the two regimes lies in the relative sizes of L and $(\nu t)^{\frac{1}{2}}$. It is reassuringly consistent that inserting the condition $L \sim (\nu t)^{\frac{1}{2}}$ into either (A 5) or (A 7) leads to the same result: the Stokes flow analysis will hold if

$$\left.\begin{aligned} t &\gg \left(\frac{g'^2Q^4}{\nu^{2n+5}}\right)^{1/(2n+1-4\alpha)} \quad \left(\alpha < \frac{2n+1}{4}\right), \\ t &\ll \left(\frac{g'^2Q^4}{\nu^{2n+5}}\right)^{1/(2n+1-4\alpha)} \quad \left(\alpha > \frac{2n+1}{4}\right), \\ \text{or} \quad \frac{g'^2Q^4}{\nu^{2n+5}} &\ll 1 \quad \left(\alpha = \frac{2n+1}{4}\right), \end{aligned}\right\} \tag{A 9}$$

and the boundary-layer analysis will hold if the converse conditions are satisfied. The same conclusions may, of course, be obtained by a comparison of the magnitudes of the inertial and viscous forces. Our final requirement, that $H \ll L$, may be shown to reduce to

$$t \gg \left(\frac{\nu^{n+2}}{Qg'^{n+2}}\right)^{1/(\alpha+n+2)} \quad \text{(Stokes flow)}, \tag{A 10a}$$

$$t \gg \left(\frac{\nu}{g'^2}\right)^{\frac{1}{3}} \quad \text{(boundary layer flow)}. \tag{A 10b}$$

In the derivation of (A 6) to describe flow over a shallow layer we assumed that $H \ll d$ and that $d \ll L$. From (A 6) and (A 1) we may deduce that the first of these conditions requires

$$\left.\begin{aligned} t &\gg \left(\frac{Q^2\nu^{n+1}}{g'^{n+1}d^{3n+5}}\right)^{1/(n+1-2\alpha)} \quad \left(\alpha < \frac{n+1}{2}\right), \\ t &\ll \left(\frac{Q^2\nu^{n+1}}{g'^{n+1}d^{3n+5}}\right)^{1/(n+1-2\alpha)} \quad \left(\alpha > \frac{n+1}{2}\right), \\ \text{or} \quad & \frac{Q^2\nu^{n+1}}{g'^{n+1}d^{3n+5}} \ll 1 \qquad \left(\alpha = \frac{n+1}{2}\right). \end{aligned}\right\} \tag{A 11}$$

The constraint will be satisfied at sufficiently large times if $\alpha < \frac{1}{2}$ (two-dimensional) or $\alpha < 1$ (axisymmetric). If α exceeds these values then the depth of intruding fluid will increase with time until it touches the rigid boundary at the base of the shallow layer; the analysis leading to (A 8) will then be appropriate. If α equals these values then the scalings (A 6) and (A 8) are equivalent. A detailed mathematical description for this case is given in Appendix B.

The restriction that $d \ll L$ is easily seen from (A 6) to be satisfied at large times. At very short times, when $L \ll d$, the layer of ambient fluid appears deep and (A 5) or (A 7) may be applicable. The final condition for the validity of (A 6) is the neglect of inertial effects. This may be evaluated by a comparison of the magnitude of inertial and viscous forces. More simply, we note that inertial effects will be negligible if the timescale of the motion is much greater than the viscous diffusion timescale based on the layer depth, i.e.

$$t \gg \frac{d^2}{\nu}. \tag{A 12}$$

A.2. *Diffusion*

Consider an intrusion spreading in accordance with one of equations (A 5)–(A 8). Suppose, for definiteness, that the upper fluid is immiscible with the other two and that the density difference between the lower fluid and the intruding fluid is due to a diffusive property (heat or composition) with diffusivity κ. The effects of diffusion will be negligible provided that the intrusion is much thicker than the diffusive boundary layer; that is $H \gg (\kappa t)^{\frac{1}{2}}$. The time at which $H \sim (\kappa t)^{\frac{1}{2}}$ may readily be estimated from (A 1) and (A 5)–(A 8). Thereafter, diffusion of density differences is as important as advection and the vertical extent of the intrusion is given by

$$H \sim (\kappa t)^{\frac{1}{2}}. \tag{A 13}$$

The thickening of the intrusion by diffusion causes the volume of fluid in the intrusion to be greater than Qt^α. Therefore, (A 1) must be replaced by the statement that total buoyancy is conserved. Thus, the effective value of g' is reduced from its initial non-diffusive value g'_0 owing to the dilution of the stratifying species. Hence

$$g'_{\text{eff}} = \frac{Qt^\alpha}{L^{n+1}(\kappa t)^{\frac{1}{2}}} g'_0. \tag{A 14}$$

Equating the buoyancy and viscous forces given by (A 3) and (A 4) yields

$$g'_{\text{eff}} H^2 \sim \frac{\nu L^2}{Dt}. \tag{A 15}$$

The spreading law for the diffusive intrusion can then be obtained by substitution of the appropriate estimate of D, and of the values of $g'_{\rm eff}$ and H from (A 13) and (A 14), into (A 15). The results are summarized in table 2. We note that Q and g'_0 only occur as their product since it is the buoyancy flux, rather than the initial volume of the intruding fluid, that determines the rate of spread in the diffusive regime.

In each case, there are conditions for the validity of these spreading laws. For a diffusion-dominated intrusion of vertical extent given by (A 13) we require $Qt^{\alpha}/L^{n+1} \ll (\kappa t)^{\frac{1}{2}}$. The conditions for the separation of scales ($H \ll L$ (all cases), $H \ll d \ll L, (\nu t)^{\frac{1}{2}}$ (shallow layer), $L \ll (\nu t)^{\frac{1}{2}}$ (Stokes flow) and $L \gg (\nu t)^{\frac{1}{2}}$ (boundary layer)) are analogous to those applicable to non-diffusive intrusions. Each of these conditions may easily be rearranged using the expressions in table 2 to give the range of t for which the spreading law is appropriate. Since the viscous diffusion scale $(\nu t)^{\frac{1}{2}}$ must in each case be greater than the buoyancy diffusion scale $(\kappa t)^{\frac{1}{2}}$, the Prandtl number must satisfy $Pr \gg 1$.

A.3. *Surface tension*

Suppose now that the fluids in the upper and lower layers and the intrusion are all immiscible. Let σ_{+-}, σ_{+0} and σ_{-0} be the coefficients of interfacial tension between the fluids and let $\sigma = \sigma_{+-} - \sigma_{+0} - \sigma_{-0}$. Then the total force due to surface tension is given by

$$F_{\rm s} \sim \sigma L^n. \tag{A 16}$$

If $\sigma < 0$ then we look for a quasi-steady equilibrium in which there is a surface tension-buoyancy balance. From (A 3) and (A 16) we recover the result that such a balance requires spreading at a constant thickness given by

$$H \sim \left(\frac{|\sigma|}{\rho g'}\right)^{\frac{1}{2}} \tag{A 17a}$$

and derive the corresponding spreading rate

$$L \sim \left(\frac{\rho g' Q^2 t^{2\alpha}}{|\sigma|}\right)^{1/(2n+2)} \tag{A 17b}$$

Hence, by comparing (A 17) with (A 5)–(A 8), we see that if α is less than a critical value then there is a transition time, with corresponding lengthscale, at which a viscous–buoyancy balance is succeeded by a surface tension–buoyancy balance.

Conversely, if $\sigma > 0$ then we look for a balance between a driving surface-tension force and a retarding viscous drag. From (A 4) and (A 16),

$$Dt\sigma \sim \mu L^2. \tag{A 18}$$

The spreading relations, resulting from substitution of the relevant estimates of D, are summarized in table 2. These relations will be appropriate when the buoyancy force is negligible compared with the force due to surface tension. Results in this viscous–surface tension regime have important applications to the spread of a crude oil slick on water (Hoult 1972).

A.4. *Strong stratification*

As our final illustration of the diversity of situations that can be treated by simple scaling analyses, we consider intrusion at the neutral buoyancy level into a continuously stratified environment with buoyancy frequency N. If the stratification is strong (more precisely $Gr = N^2L^4/\nu^2 \gg 1$) then the vertical scale D of the motion

	Stokes flow	Boundary-layer flow	Flow over a shallow layer	Flow over a rigid boundary
Vertical extent of flow	$D \sim L$	$D \sim (\nu t)^{\frac{1}{2}}$	$D \sim d$	$D \sim H$
Non-diffusive intrusions				
(two-dimensional)	$L \sim \left(\frac{g'Q^2}{\nu}\right)^{\frac{1}{5}} t^{(2\alpha+1)/3}$	$L \sim \left(\frac{g'^2Q^4}{\nu}\right)^{\frac{1}{6}} t^{(4\alpha+3)/8}$	$L \sim \left(\frac{g'Q^2d}{\nu}\right)^{\frac{1}{4}} t^{(2\alpha+1)/4}$	$L \sim \left(\frac{g'Q^3}{\nu}\right)^{\frac{1}{5}} t^{(3\alpha+1)/5}$
(axisymmetric)	$L \sim \left(\frac{g'Q^2}{\nu}\right)^{\frac{1}{5}} t^{(2\alpha+1)/5}$	$L \sim \left(\frac{g'^2Q^4}{\nu}\right)^{\frac{1}{12}} t^{(4\alpha+3)/12}$	$L \sim \left(\frac{g'Q^2d}{\nu}\right)^{\frac{1}{6}} t^{(2\alpha+1)/6}$	$L \sim \left(\frac{g'Q^3}{\nu}\right)^{\frac{1}{6}} t^{(3\alpha+1)/8}$
Diffusive intrusions				
(two-dimensional)	$L \sim \left(\frac{g_0'^2Q^2\kappa}{\nu^2}\right)^{\frac{1}{4}} t^{(2\alpha+3)/4}$	$L \sim \left(\frac{g_0'^2Q^2\kappa}{\nu}\right)^{\frac{1}{6}} t^{(\alpha+2)/3}$	$L \sim \left(\frac{g_0'^2Q^2d^2\kappa}{\nu^2}\right)^{\frac{1}{6}} t^{(2\alpha+3)/6}$	$L \sim \left(\frac{g_0'Q\kappa}{\nu}\right)^{\frac{1}{3}} t^{(\alpha+2)/3}$
(axisymmetric)	$L \sim \left(\frac{g_0'^2Q^2\kappa}{\nu^2}\right)^{\frac{1}{6}} t^{(2\alpha+3)/6}$	$L \sim \left(\frac{g_0'^2Q^2\kappa}{\nu}\right)^{\frac{1}{8}} t^{(\alpha+2)/4}$	$L \sim \left(\frac{g_0'^2Q^2d^2\kappa}{\nu^2}\right)^{\frac{1}{8}} t^{(2\alpha+3)/8}$	$L \sim \left(\frac{g_0'Q\kappa}{\nu}\right)^{\frac{1}{4}} t^{(\alpha+2)/4}$
Surface-tension spreading	$L \sim \frac{\sigma t}{\mu}$	$L \sim \left(\frac{\sigma^2t^3}{\rho^2\nu}\right)^{\frac{1}{4}}$	$L \sim \left(\frac{d\sigma t}{\mu}\right)^{\frac{1}{2}}$	—

TABLE 2. Asymptotic spreading relations. In the right-hand column ν refers to the viscosity of the intruding fluid rather than that of the ambient fluid

will be equal to the vertical scale H of the force exerted by the intrusion. To make the analogy between the discontinuously stratified problem and the continuously stratified problem, we replace g' by N^2H in (A 3). A viscous–buoyancy balance of forces is then possible if

$$L \sim \left(\frac{Q^4N^2}{\nu}\right)^{1/(4n+6)} t^{(4\alpha+1)/(4n+6)} \tag{A 19}$$

(Chen 1980). For the subcase $\alpha = 1, n = 0$ this result was given previously by Maxworthy (1972).

Appendix B. Shallow-layer intrusions of constant thickness

For an intrusion of volume Qt^α spreading over a shallow layer of fluid, we showed earlier that there is a critical value of α given by $\alpha_2 = 1/(n+1)$, where $n = 0$ for a two-dimensional current and $n = 1$ for an axisymmetric current. If $\alpha < \alpha_2$ then at large times the ambient layer is much thicker than the intrusion and the solution given in §2.2 is applicable; if $\alpha > \alpha_2$ then at large times the intrusion is much thicker than the ambient layer and the solution given by Huppert (1982) is applicable. In this Appendix we derive the solution for the transition case $\alpha = \alpha_2$.

Let the geometry be as shown in figure 1 (*b*) except in that $z = 0$ is now defined to coincide with the rigid lower boundary and d is now a function of t and the horizontal coordinate x. Let $d \to d_\infty$ as $xt^{-\frac{1}{2}} \to \infty$, An appropriate hydrostatic pressure is given by

$$p_{\rm H} = p_0 - \rho_+ gz \qquad (z > h+d), \tag{B 1a}$$

$$p_{\rm H} = p_0 - \rho_0 gz + (\rho_0 - \rho_+) g(h+d) \qquad (h+d > z > d), \tag{B 1b}$$

$$p_{\rm H} = p_0 - \rho_- gz + (\rho_0 - \rho_+) gh + (\rho_- - \rho_+) gd \qquad (d > z > 0). \tag{B 1c}$$

Therefore, in $x < x_{\rm N}$

$$\frac{\partial^2 u_0}{\partial z^2} = \frac{g''}{\nu_0}\frac{\partial}{\partial x}(h+d) \qquad (h+d > z > d), \tag{B 2a}$$

$$m\frac{\partial^2 u_-}{\partial z^2} = \frac{g''}{\nu_0}\frac{\partial}{\partial x}(h+rd) \qquad (d > z > 0), \tag{B 2b}$$

where $m = \mu_-/\mu_0$, $r = (\rho_- - \rho_+)/(\rho_0 - \rho_+)$ and $g'' = g(\rho_0 - \rho_+)/\rho_0$. Equations (B 2) are solved subject to the conditions of no-slip at $z = 0$, zero stress at $z = h+d$ and continuity of velocity and stress at $z = d$. (The stress exerted by the overlying fluid may be neglected as in §2.2.) It is natural to define similarity variables by

$$\xi = \xi_{\rm N}^{-1}\left(\frac{d_\infty}{Q}\right)^{1/(n+1)} xt^{-\frac{1}{2}}, \quad H(\xi) = \frac{h(x,t)}{d_\infty}, \quad D(\xi) = \frac{d(x,t)}{d_\infty}. \tag{B 3}$$

In terms of these variables, the local and global conservation equations may be shown to reduce to

$$3mq^2\xi^{n+1}H' + \{\xi^n H[2H(3D+mH)(H'+D') + 3D^2(rD'+H')]\}' = 0 \quad (\xi < 1), \tag{B 4a}$$

$$3mq^2\xi^{n+1}D' + \{\xi^n D^2[2D(rD'+H') + 3H(H'+D')]\}' = 0 \quad (\xi < 1), \tag{B 4b}$$

$$3mq^2\xi^{n+1}D' + 2r\{\xi^n D^3 D'\}' = 0 \quad (\xi > 1), \tag{B 4c}$$

$$\xi_{\rm N} = \left(\int_0^1 (2\pi\xi)^n H\,{\rm d}\xi\right)^{-1/(n+1)}, \tag{B 5}$$

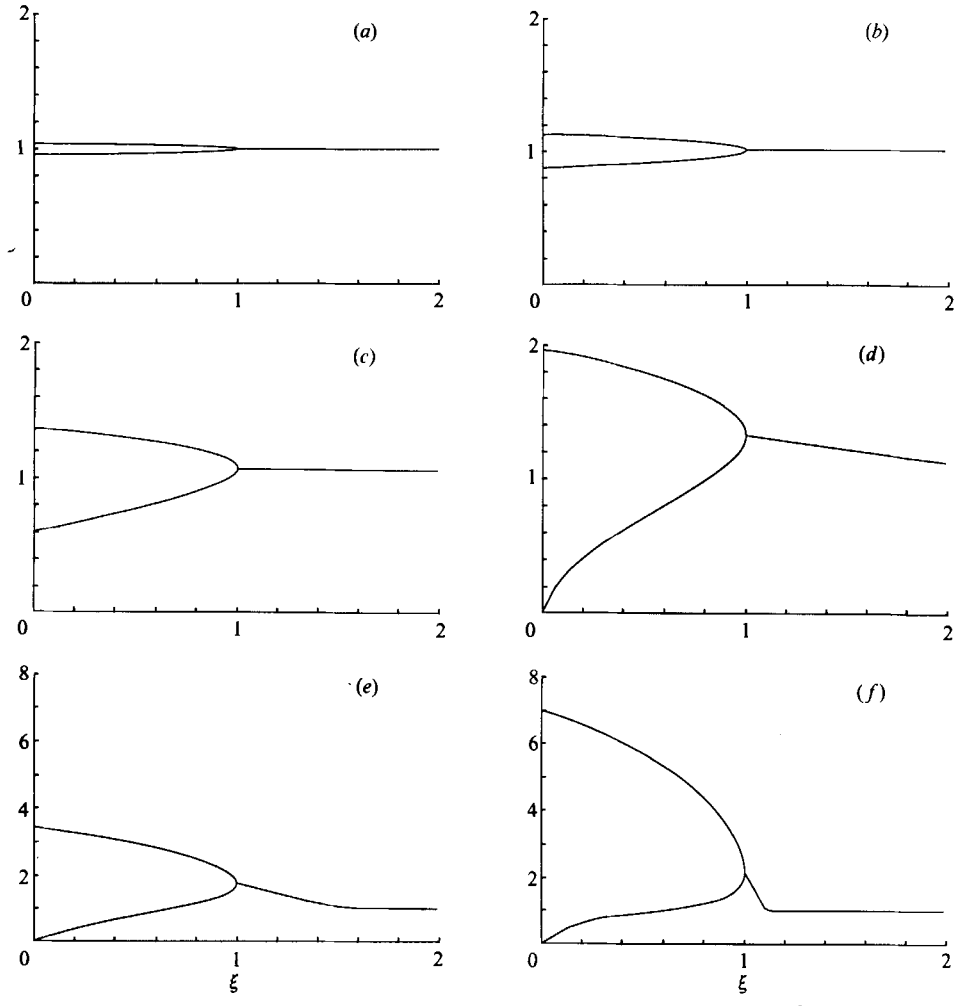

FIGURE 11. A two-dimensional gravity current, of volume proportional to $t^{\frac{1}{2}}$, spreading over a shallow layer of viscous fluid; $m = 1$ (equal viscosities) and $r = 2$ (equal density differences). For small values of the dimensionless volume flux q the current approximates spread over a shallow layer of constant depth; for large values of q the current approximates spread over a rigid surface. (*a*) $q^2 = 0.001$, (*b*) 0.01, (*c*) 0.1, (*d*) 1.0, (*e*) 10, (*f*) 100.

where the dimensionless volume flux q is defined by

$$q^2 = \left(\frac{Q^2}{d_\infty^{3n+5}}\right)^{1/(n+1)} \frac{\xi_N^2 \nu_0}{g''}. \tag{B 6}$$

The boundary conditions for (B 4) are less obvious than those for a very shallow intrusion. It is clear that both D and the flux of lower fluid must be continuous at $\xi = 1$ and that $D \to 1$ as $\xi \to \infty$. Since the total volume of lower fluid is constant there must be zero flux of lower fluid at $\xi = 0$. The condition that $H(1) = 0$ then closes the problem. Given the values of D and D' at $\xi = 1_+$, it is possible to integrate numerically from $\xi = 1$ in either direction. A shooting method can be used to find the values that enable the conditions at the origin and infinity to be satisfied.

As would be expected, it may be shown analytically that in the limit $q \to 0$ the solution approaches that of (2.29) and (2.35) and that in the limit $q \to \infty$ the solution

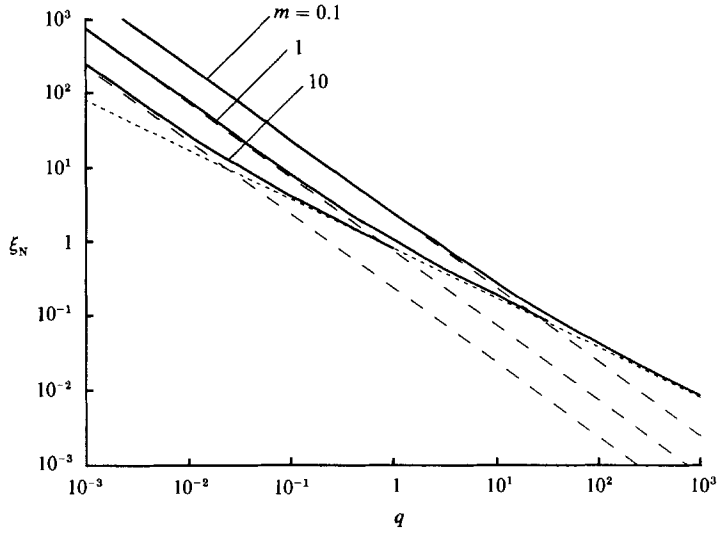

FIGURE 12. The dimensionless length $\xi_N = x_N d_\infty/(Qt^{\frac{1}{2}})$ of a two-dimensional gravity current spreading over a shallow layer of viscous fluid; $r = \infty$. The dashed asymptotes are calculated from (2.35) and correspond to the assumption that the thickness of the current can be neglected; the dotted asymptote is calculated from Huppert (1982, equation (2.13)) and corresponds to the assumption that the thickness of the ambient layer can be neglected.

approaches that of Huppert (1982, equations (2.13) and (2.25)). Some numerical solutions showing the variation in shape of a two-dimensional intrusion with q are shown in figure 11. It may be noted that at any fixed position in (real) space the intrusion is thickening. This causes an outward flux of the lower fluid and an elevation of the interface in $\xi > 1$. It is also worth commenting that if q exceeds a critical value (which depends on m and r) then the depth of the lower layer increases linearly from zero in the neighbourhood of $\xi = 0$. The variation of ξ_N with q is shown in figure 12. The asymptotic behaviour for small and large q may again be seen.

Appendix C. Numerical solution of Stokes flow integral equations

In §2.1 we showed that the equations of motion for the intrusion of one viscous fluid into an unbounded volume of another could be expressed in self-similar form. We noted that, except in the special case $\alpha = 0$, the equations for the similarity solution, (2.12) and (2.22), had no analytic solution and needed to be solved numerically. In this Appendix we describe the numerical scheme used in our calculations. The scheme is of mathematical interest owing to the care that is needed in the treatment of the singularities that arise.

Equations (2.12) and (2.22) have similar structures. To enhance this similarity and set up a convenient framework for subsequent analysis we define

$$f(x) = \left(\frac{2n+3}{2\alpha+1}\right)^{\frac{1}{2}} H(x), \tag{C 1a}$$

$$\beta = \frac{(2n+3)\,\alpha}{2\alpha+1}, \tag{C 1b}$$

$$h(x) = x + \frac{\beta}{x^n f(x)} \int_x^1 t^n f(t)\,\mathrm{d}t \quad (x \in (0,1)), \tag{C 1c}$$

where $n = 0$ for a two-dimensional current and $n = 1$ for an axisymmetric current. Then substituting and integrating once, we obtain

$$\int_0^1 ff'\mathscr{K}(t;x)\,\mathrm{d}t + h(x) = 0 \quad (x \in (0,1)), \tag{C 2}$$

where $\mathscr{K}(t;x)$ is defined by (2.9) in an axisymmetric geometry and is equal to $(1/4\pi)\ln|(t+x)/(t-x)|$ in a two-dimensional geometry. In the derivation of the latter expression from (2.20) we used the oddness of the function ff' to convert the integral from the range $(-1,1)$ to the range $(0,1)$.

In either geometry, $\mathscr{K}(t;x)$ has a logarithmic singularity at $t = x$. Since $f(1) = 0$ and $h(x)$ varies linearly near $x = 1$, a consequence of this singularity is that $ff' \sim (1-t)^{-\frac{1}{2}}$ as $t \to 1$. A further (integrable) singularity arises in $f(t)$ at $t = 0$ when $\beta \neq 0$, owing to the continual introduction of fluid at the origin. It is the careful analysis of these three singularities, at $t = 0$, x and 1, that presents the principal challenge in the solution of (C 2). A numerical scheme should not only take care of the infinities, but should do so efficiently if an excessive number of points is not to be required to obtain an accurate discretization of the problem.

Integration by parts from $t = x$ reduces the singularity at $t = 1$ to $(1-t)^{\frac{1}{2}}$ and makes the singularity at $t = x$ removable. We let $z(x) = \frac{1}{2}f^2(x)\,(1-x^2)^{-\frac{1}{2}}$ and, after some algebra, obtain

$$\gamma x z(x) + \int_0^1 (z(t)-z(x))\,(1-t^2)^{\frac{1}{2}}\mathscr{K}'(t;x)\,\mathrm{d}t = h(x), \tag{C 3}$$

where $\gamma = \frac{1}{16}\pi$ (axisymmetric) and $\gamma = \frac{1}{4}$ (two-dimensional). Considerable simplification in (C 3) was gained by use of the identity

$$(1-x^2)^{\frac{1}{2}}\mathscr{K}(1) + \int_0^1 ((1-t^2)^{\frac{1}{2}} - (1-x^2)^{\frac{1}{2}})\,\mathscr{K}'(t)\,\mathrm{d}t = \gamma x \tag{C 4}$$

derived from the particular solution of (C 2) in which $z(x)$ is found to be constant when $\alpha = 0$ (2.15) and (2.23)). Our aim now is to represent $z(t)$ in (C 3) by n values $z_i \equiv z(x_i), 0 < x_1 < x_2 < \ldots < x_n = 1$, to find a discrete representation of the integral for each x_i as a linear combination of $\{z_i\}$, and then to solve the resulting system of linear equations for $\{z_i\}$ as a function of $\{h_i \equiv h(x_i)\}$.

The most elegant way of dealing with the non-polynomic nature of the integrand at $t = 0$ and $t = 1$ is to write it as the product of a general polynomic function and a simple weighting function with the appropriate singularities (see e.g. Acton 1970). It is then straightforward to deduce an integration rule that is an identity when the degree of the polynomial is less than a specified number. The extraction of the factor $(1-x^2)^{\frac{1}{2}}$ in the definition of $z(x)$, as well as allowing use of the simplifying identity (C 4), was also the first application of this 'product-integral' method and ensured that $z(x)$ is well-behaved at $x = 1$. The second application takes care of the singularity in $z(t)$ at $t = 0$.

Consider the singularity in $f(x)$ at $x = 0$. In the axisymmetric case suppose $f(t) \sim t^p$, $-1 < p < 0$, as $t \to 0$. Therefore $ff' \sim t^{2p-1}$. Since $\mathscr{K}(t;x) = \mathscr{K}(at;ax)\,\forall a$ then $\int_0^1 ff'\mathscr{K}\,\mathrm{d}t \sim x^{2p}$ as $x \to 0$. But $h(x) \sim x^{-p-1}$ so from (C 2) $p = -\frac{1}{3}$. Consider now the two-dimensional case and suppose that $f(0)$ is finite. Then $h(0) > 0$ and from (C 2) and the properties of Hilbert transforms we deduce that $f^2 \sim \ln x$, contradicting our original assumption that $f(0)$ is finite. However, if $f^2 \sim \ln x$ (or is more singular) then $h(0) > 0$ and so $f(0)$ is finite! We conclude that f^2 must be singular at the origin but less so than $\ln x$.

Following the indications above we define a weight function $w(t)$ by

$$w(t) = t^{-\frac{2}{3}} \quad \text{(axisymmetric)}, \tag{C 5a}$$

$$w(t) = \ln t \quad \text{(two-dimensional)}, \tag{C 5b}$$

and approximate $z(t)$ by $aw(t)+b$, where a and b are constants on each interval (x_i, x_{i+1}) and are chosen so that the approximant agrees with the two nearest members of $\{z_i\}$. (The more obvious alternative, $(at+b)\,w(t)$, does not allow for the fact that f becomes well-behaved as $\alpha \to 0$.) Let

$$\left.\begin{aligned} e_{ik} &= \int_{I_k} (1-t^2)^{\frac{1}{2}} \mathscr{K}'(t; x_i)\,(w(t)-w_k)\,\mathrm{d}t/(w_{k+1}-w_k) \\ f_{ik} &= \int_{I_k} (1-t^2)^{\frac{1}{2}} \mathscr{K}'(t; x_i)\,(w_{k+1}-w(t))\,\mathrm{d}t/(w_{k+1}-w_k) \end{aligned}\right\} \tag{C 6}$$

where $I_k = (x_k, x_{k+1})$ for $k \geqslant 2$ and $I_1 = (0, x_2)$.

This defines a discrete approximation to (C 3) by

$$h_i = \left(\gamma x_i - \sum_{k=1}^{n-1} (e_{ik}+f_{ik})\right) z_i + \sum_{k=1}^{n-1} (e_{ik}\, z_{k+1} + f_{ik}\, z_k) \tag{C 7}$$

which may be inverted to give $\{z_i\}$ in terms of $\{h_i\}$ and the numerical coefficients e_{ik} and f_{ik}.

The integrals $e_{ik}\,(i = k+1)$ and $f_{ik}\,(i = k)$ are singular but enter (C 7) with identically zero weight and may be ignored. In the remaining integrals the bad behaviour in $(1-t^2)^{\frac{1}{2}}$ may be eliminated by the substitution $t = \sin\theta$, and the singularities in $e_{ik}\,(i = k)$ and $f_{ik}\,(i = k+1)$ are removable. The singularity of $w(t)$ at $t = 0$ is avoided by making the substitution $t = u^3$ (axisymmetric) or by integration by parts (two-dimensional) when $k = 1$. These final manipulations represent e_{ik} and f_{ik} as integrals of polynomic functions and simple application of Simpson's rule will evaluate them to high accuracy.

The calculation of $h(x)$ from $\{z_i\}$ using (C 1c) proceeds in a similar fashion. We define

$$g(x) = x^n (2z(1+x)^{\frac{1}{2}})^{\frac{1}{2}} \tag{C 8}$$

and approximate $g(t)$ in a manner analogous to $z(t)$. This generates an approximation to (C 1c) of the form

$$\left.\begin{aligned} h_n &= 1, \\ h_i &= x_i + \frac{\beta}{g_i (1-x_i)^{\frac{1}{4}}} \sum_{k=i}^{n-1} (p_k\, g_k + q_k\, g_{k+1}) \quad (i < n), \end{aligned}\right\} \tag{C 9}$$

with numerical coefficients p_i and q_i.

We may now use this formalism to define an iterative numerical scheme to solve (2.12) and (2.22) for a range of values of α. The computation of the numerical coefficients e_{ik} and f_{ik} and the inversion of (C 7) is the most expensive part of the calculation. Since these are independent of α and $f(x)$ they may be moved out of the iterative loop to provide the following efficient scheme:

calculate e_{ik}, f_{ik}, p_i, q_i;
calculate the inverse matrix for (C 7);
define $\{g_i\}$ *from* $\alpha = 0$ *solution*;

for $\alpha = 0$ **to** α_{max} **step** $\Delta\alpha$ **do**
begin repeat *calculate* $\{h_i\}$ *from* $\{g_i\}$ *using* (C 9);
calculate $\{z_i\}$ *from* $\{h_i\}$ *using inverse matrix*;
calculate $\{g_i\}$ *from* $\{z_i\}$ *using* (C 8);
until *convergence to desired accuracy attained*;
end.

This scheme converged for all values of α tried; the rate of convergence could be increased by a suitable amount of under- or over-relaxation when updating $\{g_i\}$. The results are shown in figures 2 and 3.

We conclude with formulae for the axisymmetric kernel $\mathscr{K}(t;x)$ derived from results given by Lee & Leal (1982). From (2.9) we deduce

$$\mathscr{K}(t;x) = \frac{1}{4\pi}\left(\left(1+\frac{t}{x}\right)(\mathrm{K}-\mathrm{E})-\frac{2t}{x+t}\mathrm{K}\right), \tag{C 10a}$$

$$\mathscr{K}'(t;x) = \frac{t}{4\pi x}\left(\frac{\mathrm{E}}{x-t}+\frac{\mathrm{K}}{x+t}\right), \tag{C 10b}$$

where K and E are the complete elliptic functions of the first and second kinds with argument $m = 4tx/(x+t)^2$.

REFERENCES

Acton, F. S. 1970 *Numerical Methods That Work*. Harper & Row.

Britter, R. E. & Simpson, J. E. 1978 Experiments on the dynamics of a gravity current head. *J. Fluid Mech.* **88**, 223–240.

Chen, J.-C. 1980 Studies on gravitational spreading currents. *Rep.* KH-R-40, California Institute of Technology.

Didden, N. & Maxworthy, T. 1982 The viscous spreading of plane and axisymmetric gravity currents. *J. Fluid Mech.* **121**, 27–42.

Fay, J. A. 1969 The spread of oil slicks on a calm sea. In *Oil on the Sea* (ed. D. P. Hoult), pp. 53–63. Plenum.

Hinch, E. J. 1972 The mechanics of suspensions. Ph.D. thesis, Cambridge Univerity.

Hoult, D. P. 1972 Oil spreading on the sea. *Ann. Rev. Fluid Mech.* **4**, 341–368.

Huppert, H. E. 1982 The propagation of two-dimensional and axisymmetric viscous gravity currents over a rigid horizontal surface. *J. Fluid Mech.* **121**, 43–58.

Huppert, H. E., Shepherd, J. B., Sigurdsson, H. & Sparks, R. S. J. 1982 On lava dome growth, with application to the 1979 lava extrusion of Soufrière, St Vincent. *J. Volcanol. Geotherm. Res.* **14**, 199–222.

Huppert, H. E. & Simpson, J. E. 1980 The slumping of gravity currents. *J. Fluid Mech.* **99**, 785–799.

Jeffery, G. B. 1922 The motion of ellipsoidal particles immersed in a viscous fluid. *Proc. R. Soc. Lond.* A **102**, 161–179.

Kerr, R. C. & Lister, J. R. 1987 The spread of subducted lithospheric material along the mid-mantle boundary. *Earth Planet. Sci. Lett.* **85**, 241–247.

Ladyzhenskaya, O. A. 1963 *The Mathematical Theory of Viscous Incompressible Flow*. Gordon & Breach.

Lee, S. H. & Leal, L. G. 1982 The motion of a sphere in the presence of a deformable interface. *J. Colloid Interface Sci.* **87**, 81–106.

Maxworthy, T. 1972 Experimental and theoretical studies of horizontal jets in a stratified fluid. In *Proc. Intl Symp. on Stratified Flows, Novosibirsk*, pp. 611–618. ASCE.

Maxworthy, T. 1983 Gravity currents with variable inflow. *J. Fluid Mech.* **128**, 247–257.

Miner, C. S. & Dalton, N. N. 1953 *Glycerol*. Reinhold.

Simpson, J. E. 1982 Gravity currents in the laboratory, atmosphere and ocean. *Ann. Rev. Fluid Mech.* **14**, 213–234.